CHAPTER

7

Nuclear Interactions of High-energy Particles from Artificial Sources

7.1. ***Production and detection of high-energy nucleons.*** Electro-nuclear machines now in operation provide sources of protons and neutrons with energies up to several hundred Mev. Others, still in the development stage, will reach presumably energies of the order of several Bev.

High-energy protons are produced by direct acceleration of hydrogen nuclei. They can be obtained in the form of a well collimated and fairly mono-energetic beam.

High-energy neutrons are produced by nuclear interactions of protons or other charged particles accelerated by the machine.

Nuclear disintegrations induced by deuterons represent a convenient source of neutrons in the energy range extending from several Mev to several tens of Mev. For example, a lithium target bombarded by deuterons gives neutrons distributed in a continuous energy spectrum extending to a maximum energy that depends on the energy of the incident deuterons and on the angle of emission. The reaction is strongly exothermic and has a Q-value of about 15.2 Mev, so that, for example, deuterons of 10 Mev produce neutrons of energy up to about 23.5 Mev in the forward direction.

Neutrons of higher energies are obtained largely by the processes of *charge exchange* and of *stripping*. One describes as *charge exchange* a process in which a proton, on traversing a nucleus, transfers its charge onto a neutron and continues its course changed into a neutron, with only a comparatively small energy loss. By such a process, for example, a beryllium target bombarded with 340-Mev protons gives in the forward direction a neutron beam with a wide maximum around 260 Mev (KEL50).

Stripping is a process in which a high-energy deuteron, on traversing a nucleus, leaves the proton behind while the neutron goes on with an energy approximately equal to one-half the initial energy of the deuteron. This process was predicted theoretically by Serber (SbR47.1), who computed

the angle and the energy distribution of the resulting neutrons and protons. The theoretical predictions were confirmed by the experimental work of Helmholz and his collaborators on the angular distribution of neutrons (HAC47), and of Hadley and his collaborators on the energy distribution of neutrons (HJ49). Both theory and experiment show that neutrons obtained by the stripping process have a fairly narrow energy distribution. For example, the stripping of 190-Mev deuterons on a beryllium target gives rise, in the forward direction, to a neutron spectrum with a maximum at 90 Mev and a half-width of about 20 Mev (HJ49).

High-energy protons may be detected directly, for example, by means of proportional counters (§ 3.4) or scintillation counters (§ 3.17). For the detection of neutrons one may use any of their nuclear interactions. The simplest, in principle, is the collision of neutrons against hydrogen nuclei in a hydrogenous material. This process gives rise to proton recoils whose energy is related to the energy of the incident neutrons and to the angle of emission. Another convenient method of detection is based upon the production of radioactive isotopes by $(n,2n)$ reactions, such as the $Cu^{63}(n,2n)Cu^{62}$ reaction giving rise to a copper isotope with a 10-minute positon activity, or the $C^{12}(n,2n)C^{11}$ reaction giving rise to a carbon isotope with a 20.5-minute positon activity. Samples of the material to be activated, usually in the form of discs, are placed in the neutron beam for definite periods of time and their activity is then measured by means of Geiger-Mueller counters.

Reactions of the $(n,2n)$ type have a definite energy threshold. Thus the $Cu^{63}(n,2n)Cu^{62}$ reaction is produced only by neutrons of more than about 11 Mev and the $C^{12}(n,2n)C^{11}$ reaction by neutrons of more than about 21 Mev. This circumstance affords the possibility of experimenting on fairly mono-energetic groups of neutrons, even though the neutron source may have a continuous spectrum. For example, a Li target bombarded with 0.9-Mev deuterons gives, at 90°, neutrons with a maximum energy somewhat greater than 14 Mev. If one detects these neutrons by the activation of copper Cu^{63}, one effectively selects a narrow band of neutron energies, whose center is at approximately 14 Mev (AE46).

Still another method for the detection of neutrons makes use of their ability to produce fission. For example, an ionization pulse chamber lined with bismuth provides a convenient detector for neutrons of energy greater than about 50 Mev, this being the threshold for bismuth fission.

7.2. ***Total nuclear cross-sections for high-energy neutrons.*** Since neutrons have no electric charge, their electromagnetic interactions are extremely weak.* Therefore nuclear collisions represent by far the most important interaction between high-energy neutrons and matter.

* They are not exactly zero because the neutron exists, for part of the time, as a proton plus a negative meson. This fact gives rise to the magnetic moment of the neutron and possibly to other electromagnetic effects.

Table 7.2.1. Total nuclear cross-sections for neutrons of different energies, in units of 10^{-24} cm^2 (inclusive of diffraction scattering). [From experimental data of Amaldi, *et al.*, at 14 Mev (AE46), of Sherr at 23 Mev (SR45), of Hildebrand, *et al.*, at 42 Mev (HRH50), of Cook, *et al.*, at 85 Mev (CLJ49), of De Juren, *et al.*, at 90 Mev (DJJ50.1) and at 270 Mev (DJJ50.2), and of Fox, *et al.*, at 280 Mev (FR50).]

			Effective Neutron Energy (Mev)						
Element	A	Z	14	23	42	85*	95	270	280
H	1	1		0.39	0.203 ± 0.007	0.083 ± 0.004	0.073 ± 0.0015	0.038 ± 0.0015	0.033 ± 0.003
D	2	1			0.289 ± 0.013	0.117 ± 0.005	0.104 ± 0.004		0.049 ± 0.005
Li	6.9	3			0.684 ± 0.011	0.314 ± 0.006			0.164 ± 0.007
Ba	9	4	0.65 ± 0.03		0.853 ± 0.01	0.431 ± 0.008	0.396 ± 0.004		0.225 ± 0.004
B	10.8	5	1.16 ± 0.13		0.985 ± 0.02				
C	12	6		1.29	1.089 ± 0.011	0.550 ± 0.011	0.498 ± 0.003	0.238 ± 0.003	0.279 ± 0.004
N	14	7			1.220 ± 0.025	0.656 ± 0.021	0.570 ± 0.007		
O	16	8		1.60	1.358 ± 0.012	0.765 ± 0.020	0.663 ± 0.007		0.380 ± 0.008
F	19	9			1.603 ± 0.03				
Na	23	11			1.67 ± 0.06				
Mg	24.3	12	1.83 ± 0.09		1.723 ± 0.024	1.03 ± 0.02	0.993 ± 0.011		
Al	27	13	1.92 ± 0.08	1.85	1.782 ± 0.020	1.12 ± 0.02		0.555 ± 0.008	0.566 ± 0.018
S	32.1	16	1.58 ± 0.09		1.974 ± 0.030				
Cl	35.5	17		1.88	2.11 ± 0.04	1.38 ± 0.03	1.28 ± 0.02		
Ca	40.1	20			2.210 ± 0.026				
Fe	55.8	26	2.75 ± 0.05		2.441 ± 0.021				
Ni	58.7	28	2.62 ± 0.06		2.51 ± 0.034				
Cu	63.6	29	2.86 ± 0.13	2.50	2.54 ± 0.019	2.22 ± 0.04	2.00 ± 0.03	1.15 ± 0.02	1.19 ± 0.02
Zn	65.4	30	3.03 ± 0.15		2.618 ± 0.027	2.21 ± 0.04			
Se	9.2	34	3.35 ± 0.18						
Br	79.9	35			2.93 ± 0.06				
Sr	87.6	38			2.99 ± 0.12				
Mo	96	42			3.11 ± 0.05				
Ag	107.9	47	3.82 ± 0.09	3.70	3.229 ± 0.034				
Cd	112.4	48	4.25 ± 0.07						
Sn	118.7	50	4.52 ± 0.09		3.251 ± 0.023	3.28 ± 0.06	3.18 ± 0.03		1.83 ± 0.03
Sb	121.8	51	4.35 ± 0.10						
I	126.9	53			3.51 ± 0.06				
Ba	137.4	56			3.57 ± 0.12				
Ta	180.9	73			4.20 ± 0.04				
W	183.9	74			4.31 ± 0.06				
Au	197.2	79	4.68 ± 0.9						2.80 ± 0.03
Hg	200.6	80	5.64 ± 0.19	5.25	4.51 ± 0.06				
Pb	207.2	82	5.05 ± 0.08		4.44 ± 0.05	4.53 ± 0.09	4.48 ± 0.03	2.84 ± 0.03	2.89 ± 0.03
Bi	209	83	5.17 ± 0.11		4.58 ± 0.06				
Th	232.1	90			5.03 ± 0.07				
U	238.2	92			5.12 ± 0.07	5.03 ± 0.10	4.92 ± 0.06		3.14 ± 0.05

* The neutron energy in this experiment was first given as 90 Mev. Later considerations [see ref. (FR50)] have shown that the effective energy was actually 85 Mev.

The collision of a neutron against a nucleus may result in a change of direction of its trajectory, with various degrees of energy loss, or in an absorption of the neutron by the nucleus (followed, usually, by a nuclear disintegration). The total cross-section for these different processes may be determined by a so-called "good-geometry" absorption measurement, whose principle is illustrated in Fig. 1. In this figure, S represents the

Fig. 7.2.1. Good geometry absorption measurement.

neutron source, D the detector, A the absorber. The transverse dimensions of both the source and the detector are small compared with their distance, and the transverse dimensions of the absorber are only slightly larger than those necessary to intercept the neutrons traveling from the source to the detector. With this arrangement, neutrons that either stop or undergo even small-angle deflections on traversing the absorber are taken out of the beam that reaches the detector.

By plotting the intensity, I, of the neutron beam recorded by the detector as a function of the absorber thickness, x (in g cm^{-2}), one obtains an exponential curve:

$$I(x) = I_0 e^{-x/L_c}. \tag{1}$$

The quantity L_c is called the "collision mean free path." The ratio dx/L_c represents the probability for a neutron to undergo a collision on traversing the infinitesimal thickness dx. If one assumes that each nucleus represents an obstacle with cross-sectional area σ, one can express the same probability as $(N/A)\sigma\, dx$, where N is Avogadro's number (number of nuclei per gram atom) and A the atomic mass number. The quantity σ is called the *total nuclear cross-section* and is related to L_c by the equation:

$$\sigma = \frac{A}{NL_c}. \tag{2}$$

The nuclear cross-sections depend on the neutron energy. Table 1 summarizes the results of "good-geometry" absorption measurements performed by various experimenters on neutrons of energies greater than 10 Mev. The data relative to elements that are in a gaseous state at normal temperature (e.g., hydrogen) were obtained indirectly, by comparison between the absorption of a binary compound containing the element under investigation (e.g., paraffin) and that of the other element in the compound (e.g., carbon).

One should notice that lack of mono-energetic sources of neutrons makes it necessary to refer each experimental result to an estimated *effective neutron energy*, E_{eff}, rather than to a definite neutron energy. This effective energy is defined as the energy of a mono-energetic neutron beam

for which the nuclear cross-section of a given substance has the experimentally determined value, σ_{exp}. In a formula:

$$\sigma(E_{\text{eff}}) = \sigma_{\text{exp}}.$$

In order to evaluate the effective energy one must consider the shape of the neutron spectrum as well as the energy dependence of the detector efficiency and of the cross-section investigated.

Protons, unlike neutrons, lose energy by electromagnetic interactions. For energies up to several hundred Mev, the range of a proton in matter is smaller than its mean free path for nuclear interactions. Moreover protons undergo Coulomb scattering on traversing matter. Therefore a simple "good-geometry" absorption measurement is not a suitable method for determining the cross-sections for nuclear interactions of high-energy protons.

7.3. ***Neutron-proton scattering.*** Among the absorption measurements on high-energy neutrons, those with hydrogen have greatest fundamental significance, because they yield information on the cross-section for scattering of neutrons by free protons, σ_{np}. Figure 1 summarizes the

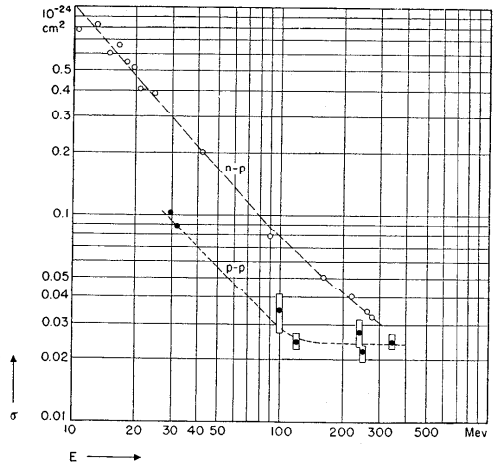

Fig. 7.3.1. The total cross-sections for n-p scattering, σ_{np}, and p-p scattering, σ_{pp}, at various energies. The experimental data for σ_{np} come from the following sources: 10.6 to 21 Mev, Sleator (SW47); 24.5 Mev, Sherr (SR45); 42 Mev, Hildebrand *et al.* (HRH50); 90 Mev, Hadley *et al.* (HJ49); 260 Mev, Kelly *et al.* (KEL50); 220 and 260 Mev, DeJuren *et al.* (DJJ51); 280 Mev, Fox *et al.* (FR50). The experimental values for σ_{pp} are based on the data summarized in Table 7.4.1.

determinations of this quantity made by various experimenters. It appears from this figure that, at neutron energies lower than about 100 Mev, the cross-section for neutron-proton scattering varies approximately in inverse proportion to the kinetic energy of the neutrons, E_n, whereas for higher energies σ_{np} seems to vary somewhat more slowly than $1/E_n$.

The scattering of a neutron by a proton (below the energy at which mesons are produced) is an elastic collision in which the neutron transfers part of its kinetic energy to the proton. The energies of the neutron and of the proton after the collision and the angles of their trajectories with respect to that of the incident neutron are correlated by equations expressing the principles of conservation of energy and momentum.

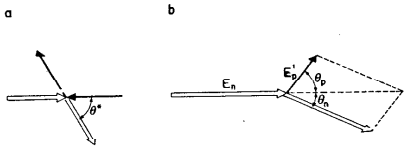

Fig. 7.3.2. Collision between a neutron and a proton: (a) in the center-of-mass system; (b) in the laboratory system.

Consider the collision both in the center-of-mass system and in the laboratory system, and refer to Fig. 2 for the explanation of the symbols used in the following discussion.

If one neglects the small difference in mass between neutrons and protons, the relative velocity, β_c, of the two frames of reference is given by Eq. (A.2.7):

$$\frac{\beta_c}{1-\beta_c^2} = \frac{p_n}{2Mc}, \tag{1}$$

where p_n is the momentum of the incident neutron in the laboratory system and M the mass of the neutron or the proton.

When $\beta_c \ll 1$, one can easily prove the following theorems:

(a) the trajectories of the proton and the neutron after the collision are at right angles with respect to one another in the laboratory system:

$$\theta_n + \theta_p = \frac{\pi}{2}. \tag{2}$$

(b) The energy, E'_p, of the secondary proton in the laboratory system is related to its angle of emission, θ_p, and to the energy, E_n, of the incident neutron by the equation:

$$E'_p = E_n \cos^2 \theta_p. \tag{3}$$

(c) The energy, E'_p, of the secondary proton in the laboratory system is related to the scattering angle, θ^*, of the neutron in the center-of-mass system by the equation:

$$E'_p = E_n \frac{1-\cos\theta^*}{2}. \tag{4}$$

In the general case (β_c not small compared with one) the following relations hold (HJ49):

$$\tan\theta_n = (1-\beta_c^2)^{1/2} \tan\frac{\theta^*}{2}; \tag{5}$$

$$\tan\theta_p = (1-\beta_c^2)^{1/2} \operatorname{cotan}\frac{\theta^*}{2}; \tag{6}$$

$$\frac{d\cos\theta_p}{d\cos\theta^*} = \frac{1}{4}\frac{1}{1-\beta_c^2}\frac{(1-\beta_c^2\cos^2\theta_p)^2}{\cos\theta_p}. \tag{7}$$

A measurement of the angular distribution of either the scattered neutrons or the recoil protons in the laboratory frame of reference determines the angular distribution of both kinds of particles in the two frames of reference. Since protons are much easier to detect than neutrons, one usually measures the angular distribution of the recoil protons. From this one then computes, by means of Eqs. (6) and (7), the angular distribution of the scattered neutrons *in the center-of-mass system*, a function of more direct theoretical significance than the observed angular distribution of protons.

In what follows, we shall describe the angular distribution of scattered neutrons in the center-of-mass system by means of the function $\psi_{np}(\theta^*)$, such that $\psi_{np}(\theta^*)\,d\omega^*$ represents the probability that, when a collision between a neutron and a proton occurs, the neutron is scattered into the solid angle $d\omega^*$ at an angle θ^* to the original direction of its motion. The quantity $\sigma_{np}\psi_{np}(\theta^*)$, where σ_{np} is the total cross-section for neutron-proton collisions, is often called the "differential scattering cross-section." The quantity $\psi_{np}(\theta^*)/L_{np}$, where L_{np} is the mean free path of neutrons in hydrogen, may be described as the differential probability for neutron-proton scattering. One will notice that $[\psi_{np}(\theta^*)/L_{np}]\,dx\,d\omega^*$ represents the probability for a neutron traversing dx g cm^{-2} of hydrogen to be deflected into the solid angle $d\omega^*$ at an angle θ^* to the direction of its initial trajectory in the center-of-mass system.

Figure 3 shows schematically a typical experimental arrangement used by Hadley, Kelly, Leith, Segrè, Wiegand, and York for the study of the angular distribution of proton recoils produced by neutrons of 40 and 90 Mev energy (HJ49). The neutron beam passes through a thin scattering foil consisting of polyethylene (CH_2) and then falls upon a bismuth fission chamber used as a monitor. The recoil protons are detected by the

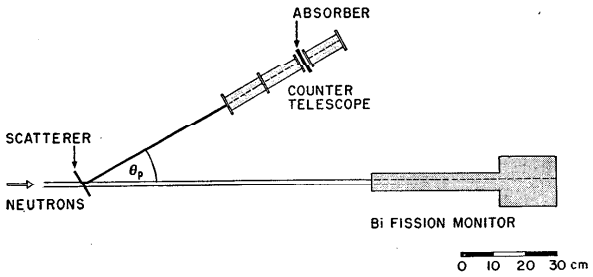

Fig. 7.3.3. Experimental arrangement for the measurement of the angular distribution of n-p scattering. From Hadley *et al.* (HJ49).

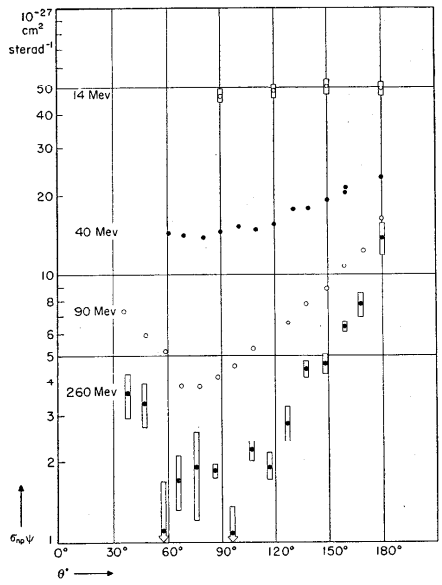

Fig. 7.3.4. The differential cross-section for n-p scattering, $\sigma_{np}\psi(\theta^*)$, in the center-of-mass system at various neutron energies. The experimental data come from the following sources: 14 Mev, Barschall *et al.* (BHH49); 40 Mev and 90 Mev, Hadley *et al.* (HJ49); 260 Mev, Kelly *et al.* (KEL50). The data at 40 Mev were normalized to a total cross-section of $2.02 \cdot 10^{-25}$ cm^2.

coincidences of a counter telescope consisting of three proportional counters placed one after the other. The common axis of these counters points to the scatterer and can be rotated with respect to the direction of the neutron beam. The proportional counters are closed at the ends with thin aluminum foils. Between the second and the third counter, however, there is an absorber, whose thickness is chosen somewhat smaller than the range of the recoil protons ejected at the angle θ_p by the neutrons under investigation. In this way the telescope is made insensitive to recoil protons produced by a possible low-energy tail of the neutron spectrum.

The results obtained in the experiment described above and in other experiments on the angular distribution of recoil protons from high-energy neutrons are summarized in Fig. 4. This figure indicates that for a neutron energy of 14 Mev the differential cross-section is practically a constant; experiments at lower neutron energies, not shown in this figure, give a similar result. At higher energies, however, the differential cross-section exhibits a minimum at around 90°. This minimum becomes more and more pronounced as the neutron energy increases. The experimental points lie on curves that do not appear to be perfectly symmetric with respect to $\theta^* = \pi/2$. The asymmetries, however, are not outside of the experimental errors. With regard to these errors one should note that the measurements become more and more difficult as the angle θ^* decreases. The reason is that as θ^* approaches zero (i.e., as θ_p approaches $\pi/2$) the energy, E'_p, of the recoil proton approaches zero.

The peak of the differential cross-section at $\theta^* = \pi$ signifies, physically, that there is a large probability for collisions in which protons are ejected in approximately the same direction and with approximately the same energy as the incident neutrons. Intuitively, one may describe this phenomenon as a *charge exchange* between a neutron in flight and a proton at rest. Indeed the fact that the cross-section is greater at $\theta^* = \pi$ than at $\theta^* = \pi/2$ is considered as strong evidence for the existence of the so-called *exchange forces* between protons and neutrons. The phenomenon mentioned in the preceding section, whereby protons change into neutrons on traversing light nuclei, is the counterpart of the effect considered here.

For a theoretical discussion of p-n scattering, the reader may consult ref. (CRS51).

7.4. *Proton-proton scattering.* For the reasons explained at the end of § 2, it has not been possible to determine the total cross-section for proton-proton scattering, σ_{pp}, by means of "good-geometry" absorption measurements of protons in hydrogenous materials. Several experimenters, however, have determined, in absolute value, the differential scattering cross-section, $\sigma_{pp}\psi_{pp}(\theta^*)$, by allowing a proton beam of known intensity to traverse thin, hydrogen-containing targets and measuring the number of protons scattered through different angles. They have used propor-

tional counters, scintillation counters, and photographic emulsions for the detection of the scattered protons.

As an example, Fig. 1 shows, schematically, the experimental arrangement used by Chamberlain, Segrè, and Wiegand (CO51) in their measurements with protons of energies between 119 and 249 Mev.

The collimated proton beam passes through an ionization chamber used as a monitor and then through a thin foil (scatterer) of hydrogenous material. The collision of a high-energy proton with a hydrogen nucleus

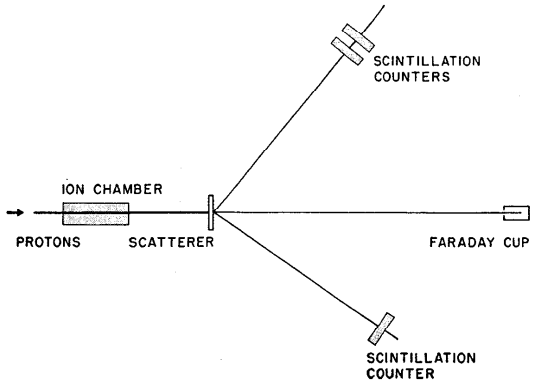

Fig. 7.4.1. Schematic diagram of an experimental arrangement for the measurement of the differential cross-section for p-p scattering.

of the target gives rise to two protons whose angles of emission are related to one another and to the energy of the incident proton by equations similar to those developed in connection with the discussion of n-p scattering (see preceding section). For a primary energy of 340 Mev, the angle between the trajectories of the two secondary protons is slightly less than 90°. In the experiment described here both secondary protons are detected, one by a telescope consisting of two crystal counters, the other by a single crystal. Calibration of the ionization chamber by means of a Faraday cup affords an absolute measurement of the proton current.

Some of the results on p-p scattering are shown in Fig. 2; others are collected in Table 1. The quantity given in both places is the differential scattering cross-section, $\sigma_{pp}\psi_{pp}(\theta^*)$, as a function of scattering angle in the center-of-mass system, θ^*. Since the two protons resulting from the collision are indistinguishable, it is convenient to define the function $\psi_{pp}(\theta^*)$ so that $\psi_{pp}(\theta^*)\, d\omega^*$ represents the probability for either proton to come

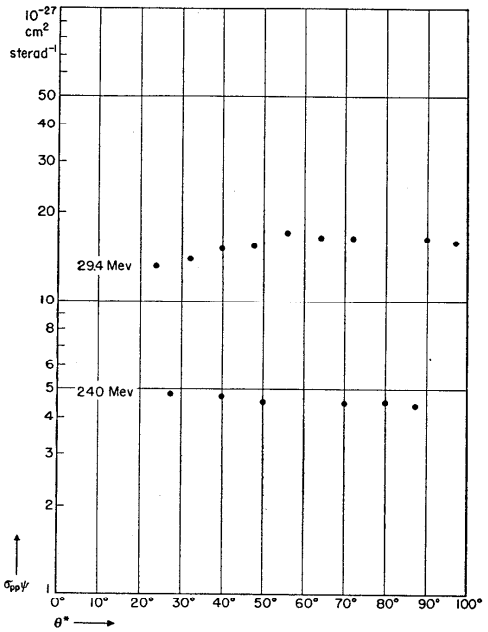

Fig. 7.4.2. The differential cross-section for p-p scattering, $\sigma_{pp}\psi(\theta^*)$, in the center-of-mass system at various proton energies. Experimental data of Panofsky *et al.* at 29.4 Mev (PWK50.2), and of Oxley at 240 Mev (private communication).

out of the collision in a direction within the solid angle $d\omega^*$ at an angle θ^* with respect to the direction of the incident proton. Thus one takes into account all possible cases by letting θ^* vary from 0 to $\pi/2$ (instead of π), and the normalizing condition for ψ_{pp} is:

$$2\pi \int_0^{\pi/2} \psi_{pp}(\theta^*) \sin \theta^* \, d\theta^* = 1. \tag{1}$$

As pointed out previously, electric forces as well as nuclear forces come into play in the collisions between two protons. In this connection we may mention here that for a primary energy near 30 Mev, Coulomb scattering becomes negligible at angles greater than about 40° in the center-of-mass system, and that for a primary energy of 340 Mev, Coulomb scattering becomes negligible at angles greater than about 7°. Figure 2 and

Table 7.4.1. The differential cross-section for p-p scattering in the center-of-mass system [$\sigma_{pp}\psi(\theta^*)$, in 10^{-27} cm^2 sterad^{-1}] for various primary energies

E_p = 29.4 Mev, from Panofsky and Fillmore (PWK50.2):

The estimated probable errors in the absolute values are ±3 per cent.

θ^* →	24°	32°	40°	48°	56°	64°	72°	80°	87°
$\sigma_{pp}\psi(\theta^*)$ →	13.2	14.0	15.2	15.6	16.7	16.3	16.5	16.4	16.0

E_p = 31.8 Mev, from Cork, Johnson, and Richman (CB50):

The estimated probable errors in the absolute values are +1.8, −1.5 per cent.

θ^* →	27.5°	40°	52°	65°	78°	90°
$\sigma_{pp}\psi(\theta^*)$ →	12.6	12.7	14.0	14.1	14.1	14.2

E_p = 100 Mev, from Birge (BRW50):

The estimated errors are of the order of 10 per cent for the relative values and of the order of 20 per cent for the absolute values.

θ^* →	41°	51°	61.5°	82°	92°
$\sigma_{pp}\psi(\theta^*)$ →	5.6	5.4	5.8	5.5	5.6

E_p = 119 Mev, from Chamberlain, Segrè, and Wiegand (CO51):

θ^* →	63°	78°	89°
$\sigma_{pp}\psi(\theta^*)$ →	4.0 ± 0.4	4.2 ± 0.4	3.95 ± 0.12

E_p = 240 Mev, private communication from C. L. Oxley.

The errors indicated refer to the relative values. The estimated error in the absolute values are of the order of 15 per cent.

θ^* →	27.5°	40°	50°	70°	80°	87°
$\sigma_{pp}\psi(\theta^*)$ →	4.8 ± 0.2	4.7 ± 0.2	4.5 ± 0.2	4.5 ± 0.1	4.5 ± 0.1	4.4 ± 0.1

E_p = 164 Mev, from Chamberlain, Segrè, and Wiegand (CO51):

θ^* →	61°	89°
$\sigma_{pp}\psi(\theta^*)$ →	4.1 ± 0.4	3.8 ± 0.3

E_p = 249 Mev, from Chamberlain, Segrè, and Wiegand (CO51):

θ^* →	48°	63°	78°	87°
$\sigma_{pp}\psi(\theta^*)$ →	3.5 ± 0.3	3.7 ± 0.2	3.09 ± 0.15	3.04 ± 0.11

E_p = 345 Mev, from Chamberlain, Segrè, and Wiegand (CO51):

Experimental values of $\sigma_{pp}\psi(\theta^*)$ ranging from 2.5 to 4.3. No clear change with angle indicated ($35° < \theta^* < 89°$).

Table 1 shows that at primary energies between 30 and 345 Mev the differential cross-section for p-p scattering in the center of mass system is approximately independent of θ^* for all values of this variable for which Coulomb scattering is negligible (at lower energies Coulomb scattering is important for most values of θ^*). Thus, at high energies, the angular distribution of p-p scattering is radically different from that of n-p scattering which, as we explained in the preceding section, becomes increasingly anisotropic with increasing energy.

The energy dependence of the scattering cross-section is also different for the two cases. In fact σ_{np} decreases steadily with increasing neutron energy, at least up to E_n = 340 Mev; σ_{pp}, instead, decreases rapidly from 30 to about 100 or 150 Mev but then remains approximately constant, at least up to 340 Mev. To illustrate this behavior we have plotted in Fig. 7.3.1 the approximate values of the total cross-section for p-p scattering at various energies, along with the values of the total cross-section for n-p scattering. The values of σ_{pp} were obtained from the available data on the differential scattering cross-section under the assumption that this quantity is independent of θ^* also for those values of θ^* at which measurements are lacking.

For a theoretical discussion of p-p scattering the reader may consult ref. (CRS51).

7.5. *Neutron-neutron scattering.* Hartsough, Hill, and Powell have described a cloud-chamber experiment on the collisions of high-energy neutrons with deuterons which, potentially at least, is capable of yielding direct information on the total cross-section for neutron-neutron scattering, σ_{nn} (HaW50; CGF50.2).

When a neutron collides with a deuteron, three different phenomena may occur: (1) the neutron may undergo elastic scattering; (2) the neutron may eject the proton from the deuteron; (3) the neutron may eject the neutron from the deuteron. When an interaction of the third type occurs, the proton that was originally part of the deuterium nucleus is left behind with a velocity equal to its instantaneous velocity at the moment of the collision. In half of the cases the proton will travel in a backward direction with respect to the incident neutron. This characterizes a collision of the third type almost unequivocally, because when the neutron collides with the proton of the deuteron (interaction of the second type) the proton is very rarely emitted at an angle of more than 90° with respect to the trajectory of the incident neutron.* Therefore one can determine the probability for neutron-neutron collisions by letting a neutron beam of known intensity traverse a cloud chamber filled with deuterium gas and observing the number of short proton tracks produced in the backward direction. The cross-section computed from these observations refers to interactions with neutrons bound to deuterons. This cross-section is somewhat different from the cross-section for collisions between two free neutrons. However, the difference is not very large and it can be estimated theoretically.

The method described above has not yet produced conclusive results. However, preliminary data obtained with 90-Mev neutrons are consistent with the assumption that the cross-section for neutron-neutron scattering

* Proton emission at an angle greater than 90° would be, of course, strictly forbidden if the target protons were at rest. The velocity of the proton in the deuteron is not sufficiently large to make the probability of this event appreciably different from zero.

equals the cross-section for proton-proton scattering, as one should anticipate theoretically.

7.6. ***A schematic nuclear model.*** Inspection of Table 7.2.1 shows that the total cross-section for nuclear scattering of high-energy neutrons varies in a regular fashion both with the energy of the neutrons and with the mass number, A, of the nucleus. In this respect, the behavior of high-energy neutrons contrasts with the behavior of neutrons in a lower range of energies, where the nuclear cross-sections show sharp resonances and vary irregularly with A. It appears that the fine details of the nuclear structure cease to be important when the neutron energy becomes larger than the binding energy of nucleons in nuclei. This suggests that one may be able to interpret the experimental results on the nuclear interactions of high-energy nucleons with nuclei on the basis of a drastically simplified picture of nuclei. In the present section we shall briefly describe a crude nuclear model that is often used for this purpose.

The probability of nuclear interactions depends primarily on the dimensions of nuclei. On the average, one can account for the properties of nuclei by assuming that a nucleus of mass number A has the shape of a sphere and that its radius, r_n, is given by the following equation:

$$r_n = r_0 A^{1/3}, \tag{1}$$

where r_0 is a constant. To be more precise, one should say that the available experimental information does not show any regular change with A in the value of the quantity r_0 defined by Eq. (1), but does not rule out small variations of r_0 from one nucleus to the other.

Note that Eq. (1) is equivalent to the assumption that the density of nuclear matter is the same for all nuclei, i.e., that the nuclear volume is proportional to the total number of nucleons in the nucleus. We wish to specify that r_n should be understood as the radius of the sphere containing the centers of the neutrons and protons that form the nucleus. In this way our definition of nuclear volume becomes independent of the delicate question concerning the "dimensions" of individual nucleons.

We shall call the area

$$\sigma_g = \pi r_n^2 = \pi r_0^2 A^{2/3} \tag{2}$$

the "geometric cross-section" of a nucleus of mass number A, and we shall refer to the corresponding mean free path,

$$L_g = \frac{A}{N\sigma_g}, \tag{3}$$

as the "geometric mean free path." In Eq. (3) N represents the number of atoms per gram-atom (Avogadro's number) and therefore L_g is measured in g cm^{-2}.

We shall neglect the interactions between the nucleons of a nucleus and account for the nuclear stability with the assumption that the nucleons are confined to the nuclear volume by very strong forces active only at the surface of this volume. In other words, we shall describe the effect of nuclear forces by assigning to the neutrons and protons a constant negative "nuclear potential energy," $-V_0$, inside the nucleus. In fairly light nuclei, containing approximately equal numbers of protons and neutrons, V_0 has practically the same value for the two kinds of particles. In heavier nuclei, containing more neutrons than protons, V_0 has presumably a somewhat greater value for the protons than for the neutrons. This conclusion is based upon the argument that the interaction energy is greater between unlike nucleons than between like nucleons.

Protons, in addition to nuclear forces, are also subject to electric forces. Outside the nucleus, the (positive) electric potential energy of a proton varies as the inverse distance from the center. Inside the nucleus it may be considered as constant in our crude model; let V_0' represent its value.

Figure 1 shows schematically the potential energies of a neutron and a proton (nuclear potential energy for the neutron, nuclear plus electric potential energy for the proton) plotted as functions of the distance from the center of the nucleus. The "potential barrier" seen by the proton is often referred to as the "Coulomb barrier."

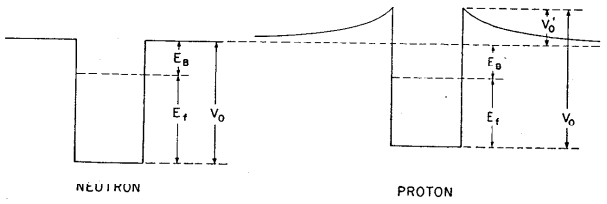

Fig. 7.6.1. Schematic representation of the potential energies of a neutron and a proton in the field of a nucleus.

Since nucleons have spin $\frac{1}{2}$, they obey Fermi's statistics; i.e., they are subject to the exclusion principle, which stipulates that each energy level cannot be occupied by more than two protons (with opposite spins) and two neutrons (also with opposite spins). The number of quantum states corresponding to momenta smaller than a given value, p, equals the available volume in phase space: $\frac{4}{3}\pi r_n^3 \cdot \frac{4}{3}\pi p^3$, divided by h^3. It follows that, in a nucleus containing Z protons and $A - Z$ neutrons, the maximum momenta, or "*Fermi momenta*," p_f, of the protons and neutrons are given by the equations:

$$\text{for protons:} \quad 2\left(\frac{4}{3}\pi\right)^2 \frac{r_n^3 p_f^3}{h^3} = Z. \qquad \text{for neutrons:} \quad 2\left(\frac{4}{3}\pi\right)^2 \frac{r_n^3 p_f^3}{h^3} = A - Z. \tag{4}$$

If one considers Eq. (1), one obtains the following values for the corresponding kinetic energies, E_f (*Fermi energies*):

$$\text{for protons:} \quad E_f = \frac{p_f^2}{2M_p} = \left(\frac{9}{32\pi^2}\right)^{2/3} \frac{h^2}{2M_p r_0^2} \left(\frac{Z}{A}\right)^{2/3}, \qquad \text{for neutrons:} \quad E_f = \frac{p_f^2}{2M_n} = \left(\frac{9}{32\pi^2}\right)^{2/3} \frac{h^2}{2M_n r_0^2} \left(\frac{A-Z}{A}\right)^{2/3}. \tag{5}$$

As we shall see in § 7.8, experimental data yield for r_0 the following approximate value:

$$r_0 \approx 1.38 \cdot 10^{-13} \text{ cm.}^* \tag{6}$$

In nuclei containing approximately equal numbers of neutrons and protons, the values of p_f and E_f are the same for the two kinds of particles. From Eqs. (5) and (6) one obtains:

$$p_f \approx 216 \text{ Mev/c}; \qquad E_f \approx 25 \text{ Mev}. \tag{7}$$

In heavy nuclei, containing appreciably more neutrons than protons, the Fermi momentum and the Fermi energy of neutrons are appreciably greater than those of protons. In lead, for example, the difference between the two values of E_f amounts to about 7 Mev.

The kinetic plus potential energy of a nucleon in the highest occupied energy level represents the *binding energy*, E_B. Thus $E_B = V_0 - E_f$ for neutrons, $E_B = V_0 - V_0' - E_f$ for protons. The binding energies of protons and neutrons are the same within about 1 Mev in any given nucleus, and do not change much from one nucleus to another. For our purposes we may take approximately $E_B \approx 8$ Mev. Equations (7) then show that for fairly light nuclei, in which $A \sim 2Z$, the value of V_0 for neutrons is approximately 33 Mev.

Notice that since in heavy nuclei E_f is smaller for protons than for neutrons, the total depth of the potential well for protons (nuclear and electric) must be smaller than the depth of the potential well for neutrons (nuclear only). Thus the effect of the Coulomb repulsion more than compensates for the somewhat greater attractive nuclear forces acting upon the protons.

One should notice that the proposed nuclear model may represent a reasonable approximation for nuclei containing fairly large numbers of nucleons but is certainly inadequate for the lightest nuclei.

* The reader should be warned that the value of r_0 is not known with as high an accuracy as the use of three digits in its expression might suggest.

7.7. Theoretical considerations on the scattering of high-energy neutrons by complex nuclei. In this section we shall apply the nuclear model described above to a discussion of the interactions of high-energy neutrons with complex nuclei.

When the energy of the incident neutron is sufficiently large, one may picture a nuclear collision as an interaction between the incident neutron and the individual nucleons of the target nucleus. According to this description, an inelastic collision occurs when the neutron, on traversing a nucleus, interacts with at least one of its nucleons. The probability of such an event depends on the cross-sections for neutron-proton and neutron-neutron scattering. Let

$$\bar{\sigma} = \frac{Z\sigma_{np} + (A - Z)\sigma_{nn}}{A} \tag{1}$$

represent the weighted average of the two cross-sections for the neutron energy under consideration. Assume that the nucleons are distributed at random in a sphere of radius r_n given by Eq. (7.6.1). Consider a neutron passing at a distance b from the center of the nucleus (see Fig. 1) and consider a circular cylinder of cross-sectional area $\bar{\sigma}$ with its axis along the trajectory of the neutron. Let Ω be the volume common to this cylinder and to the sphere representing the nucleus. Ω depends on the impact parameter, b, on the nuclear radius, r_n, and on $\bar{\sigma}$. If

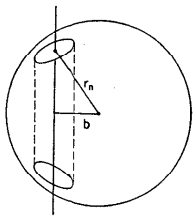

Fig. 7.7.1. Collision of a neutron against a nucleus.

$$\Omega_n = \frac{4}{3}\pi r_n^3 = \frac{4}{3}\pi r_0^3 A \tag{2}$$

represents the nuclear volume, the average number of nucleons in Ω is:

$$\frac{\Omega A}{\Omega_n} = \frac{3}{4}\frac{\Omega}{\pi r_0^3}. \tag{3}$$

According to Poisson's formula, Eq. (A.3.5), the probability that the *actual* number of nucleons in Ω is zero, i.e., the probability that no interaction occurs is $\exp(-\Omega A/\Omega_n)$. Therefore the total cross-section for inelastic collisions has the expression:

$$\sigma_i = 2\pi \int_0^{r_n + r_1} \left[1 - \exp\left(-\frac{\Omega A}{\Omega_n}\right)\right] b \, db, \tag{4}$$

where r_1 is the "interaction radius" defined by the equation:

$$\pi r_1^2 = \bar{\sigma}. \tag{5}$$

If one remembers the definition of geometric cross-section, Eq. (7.6.2), one can write Eq. (4) as follows:

$$\frac{\sigma_i}{\sigma_g} = 2\int_0^{r_n+r_1}\left[1 - \exp\left(-\frac{\Omega A}{\Omega_n}\right)\right]\frac{b}{r_n}\frac{db}{r_n}. \tag{6}$$

Since Ω/Ω_n is a function of r_1/r_n and of b/r_n, one sees that σ_i/σ_g is a function of r_1/r_n and of A.

If $r_1 \ll r_n$, Ω has, for most values of b, the approximate expression:

$$\Omega = 2\bar{\sigma}\sqrt{r_n^2 - b^2}. \tag{7}$$

The probability of traversal without collision with a nucleon becomes:

$$\exp(-\Omega A/\Omega_n) = \exp\left(-\frac{2\sqrt{r_n^2 - b^2}}{l_c}\right),$$

where $2\sqrt{r_n^2 - b^2}$ represents the "thickness of nuclear matter" traversed by the neutron, and:

$$l_c = \frac{\Omega_n}{A\bar{\sigma}} = \frac{4}{3}\frac{\pi r_0^3}{\bar{\sigma}} = \frac{1.1 \cdot 10^{-38}}{\bar{\sigma}} \tag{8}$$

represents the "collision mean free path" of the neutron in nuclear matter. In this limiting case ($r_1 \ll r_n$) Eq. (6) becomes:

$$\frac{\sigma_i}{\sigma_g} = 2\int_0^{r_n}\left[1 - \exp\left(-\frac{2\sqrt{r_n^2 - b^2}}{l_c}\right)\right]\frac{b}{r_n}\frac{db}{r_n},$$

or

$$\frac{\sigma_i}{\sigma_g} = 1 - t\left(\frac{l_c}{r_n}\right), \tag{9}$$

where:

$$t\left(\frac{l_c}{r_n}\right) = \frac{l_c^2}{2r_n^2}\left[1 - e^{-2r_n/l_c} - 2\frac{r_n}{l_c}e^{-2r_n/l_c}\right]. \tag{10}*$$

The function t physically represents the average "transparency" of the nucleus, i.e., the probability of traversal without interaction averaged over all possible paths of the neutrons through the nucleus. The dashed curve in Fig. 3 shows a graph of $1 - t = \sigma_i/\sigma_g$ plotted as a function of l_c/r_n.

Within the limits of validity of Eq. (7), the expression of the mean free path for inelastic scattering, L_i, is:

$$L_i = \frac{L_c}{1 - t(l_c/r_n)}, \tag{11}$$

* One can easily check that the approximation used here gives the correct result at the limit for values of l_c/r_n very small compared with one. In this case, Eq. (10) yields:

$$t = 1 - \frac{4}{3}\frac{r_n}{l_c}.$$

This equation, together with Eqs. (8) and (9) gives:

$$\sigma_i = A\bar{\sigma}.$$

Thus, when the mean free path in nuclear matter is very large compared with the nuclear radius, the nuclear cross-section computed according to Eqs. (9) and (10) equals the sum of the cross-sections of the individual nucleons in the nucleus. This result expresses an obvious truth.

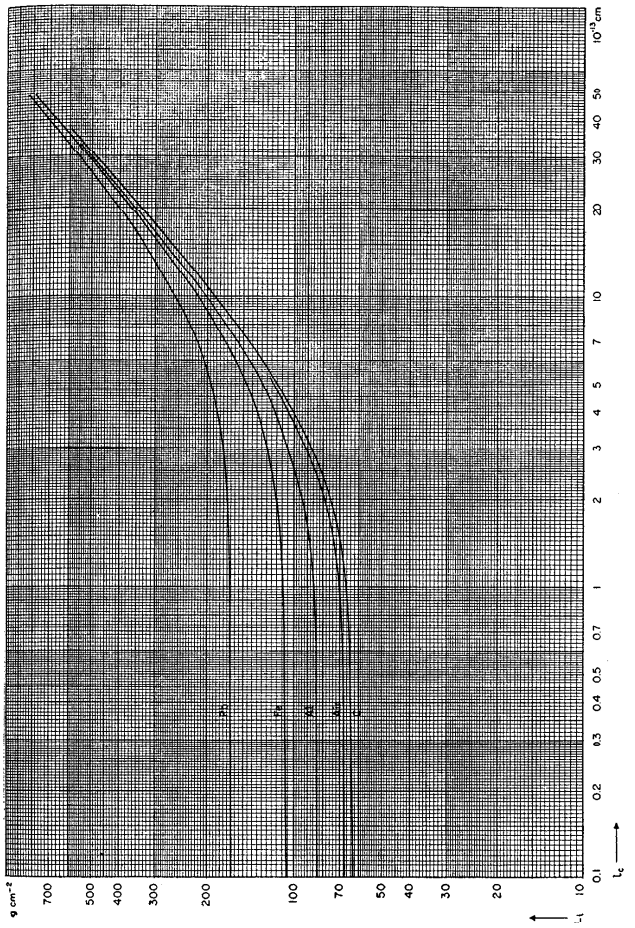

Fig. 7.7.2. The mean free paths for inelastic collision, L_i, in various substances computed from Eq. (7.7.11), and plotted as functions of the mean free path in nuclear matter, l_c.

where L_g is the geometric mean free path given by Eq. (7.6.3). The curves in Fig. 2 show the mean free paths in various substances as functions of l_c, computed from Eq. (11).

One can compute the mean free path for inelastic collisions with a different method, due to Heitler and Janossy (HtW49). This method, as we shall see later (see § 8.6), lends itself to some interesting generalizations. Let $P(x,z)\,dz$ represent the probability that a particle traveling on a straight line through a thickness x of ordinary matter traverses a total thickness between z and $z + dz$ of nuclear matter. $P(x,z)$ depends on the probability that the particle traverses a given number of nuclei and on the probability that the path length with each nucleus has a determined value.

The probability, $w(x)$, for a neutron to traverse a thickness x without undergoing an inelastic collision may be expressed, in terms of the function $P(x,z)$, as follows:

$$w(x) = \int_0^\infty P(x,z)e^{-z/l_c}\,dz, \tag{12}$$

where l_c is the collision mean free path in nuclear matter. Thus $w(x)$ is the Laplace integral of $P(x,z)$ corresponding to $\lambda = 1/l_c$, $\mathfrak{L}_P(x,1/l_c)$ see Appendix 4.

Whereas the function $P(x,z)$ has a very complicated analytic expression, its Laplace integral can be computed easily and is given by the formula:

$$w(x) = \mathfrak{L}_P\left(x,\frac{1}{l_c}\right) = e^{-x(1-t)/L_g}, \tag{13}$$

where L_g is the geometric mean free path given by Eq. (7.6.3) and t is the function defined by Eq. (10). The result expressed by Eq. (13) is equivalent to that expressed by Eq. (11). By means of the inversion formula of the Laplace integral, Heitler and Janossy were also able to obtain an approximate expression for the function P.

If r_1 is not small compared with r_n, the approximation made in the derivation of Eqs. (9) and (10) is not valid and one must compute the integral in Eq. (6) by numerical methods. This computation has been made for carbon, aluminum, iron, and lead and the results are presented, in two different forms, in Figs. 3 and 4. The solid curves in Fig. 3 give the ratio σ_i/σ_g as a function of l_c/r_n for the various elements. Figure 4 gives L_i as a function of l_c. The curves in this figure may be compared with those in Fig. 2, which were obtained from the approximate integration of Eq. (6).

This mathematical refinement of the theory has doubtful significance in view of the crude and tentative character of the nuclear model on which the theory is based.

The above computations give the cross-section for inelastic collisions of neutrons with nuclei in terms of the nuclear radius, r_n, and of the average cross-section, $\bar{\sigma}$, for n-p and n-n scattering. In the evaluation of $\bar{\sigma}$ one must consider that a neutron entering a nucleus acquires an additional kinetic energy equal to the mean (negative) potential energy, V_0, of neutrons inside a nucleus (see § 7.6). One must also allow for the effect of the exclusion principle, which forbids transition into occupied quantum states. According to Goldberger (GML48) this effect decreases the n-p and n-n cross-sections in the ratio of 1 to $[1 - (7/5)(E_f/E_n)]$, where E_n is the neutron energy and E_f is the Fermi energy (see § 7.6).

In order to discuss the experimental values of the nuclear cross-sections quantitatively it is essential to consider another phenomenon, which we have neglected so far. From the proposed model and from the general principles of wave mechanics it follows that neutrons, in addition to

inelastic scattering, must also undergo *elastic* scattering on traversing matter. This phenomenon is entirely similar to the diffraction of light by a medium containing small spheres made of an absorbing and refracting material (the index of refraction of the nucleus corresponds to the change in kinetic energy experienced by the neutrons upon entering the nucleus). In analogy with the optical effect one finds that the maximum angle of scattering is of the order of $\lambda/2r_n$, where:

$$\lambda = \frac{\hbar}{p} = 1.3 \cdot 10^{-13}\frac{Mc}{p}\ \text{cm} \tag{14}$$

is the deBroglie wave length of the neutron.

One can prove that, if the nuclei were perfectly opaque, the cross-section for elastic scattering would equal the cross-section for inelastic scattering. For partially transparent nuclei, the two cross-sections are no longer equal, but are still of the same order of magnitude. Fernbach, Serber, and Taylor (FS49) obtained general expressions for the elastic scattering cross-section in terms of the nuclear radius, the mean free path in nuclear matter, and the potential energy of neutrons in nuclei.

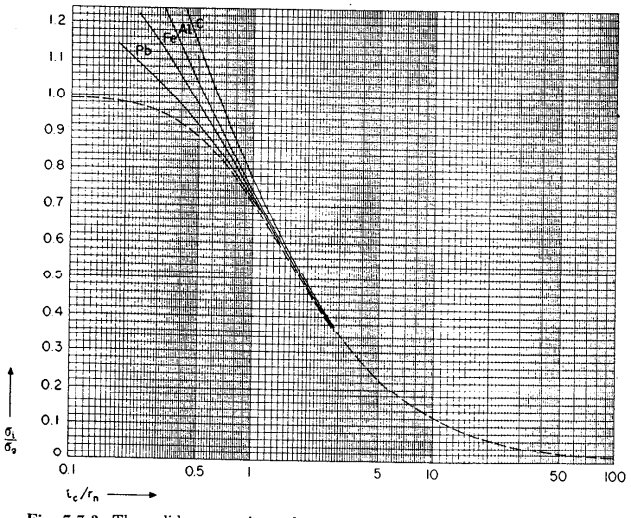

Fig. 7.7.3. The solid curves show the quantity σ_i/σ_g for carbon, aluminum, iron and lead, obtained by numerical integration of Eq. (7.7.6), and plotted as a function of l_c/r_n. The dashed curve shows the same quantity as given, for all elements, by the approximate expression (7.7.9). Computations by R. W. Safford.

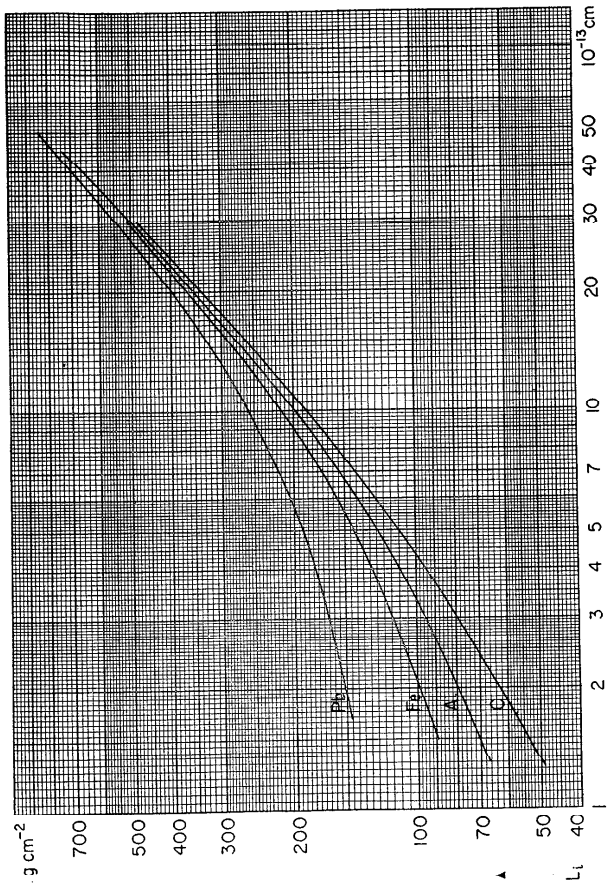

Fig. 7.7.4. The mean free paths for inelastic collisions, L_i, in various substances, computed by numerical integration of Eq. (7.7.6), and plotted as functions of the mean free path in nuclear matter, l_c. Computations by R. W. Safford.

It is hardly necessary to remark that a semiclassical approach to the problem of nuclear scattering, such as we have described above, is not very satisfactory. Indeed one should not compute the cross-section for inelastic scattering by considering the incident neutron as a material point and then add diffraction scattering to account for the wave character of the neutron, but should rather treat the neutron-nucleus interaction as a whole in the frame of wave mechanics.

Feshbach and Weisskopf (FH49) have done this under the assumption that nuclei are perfectly opaque spheres, an assumption fairly well justified at energies of the order of 10 Mev or lower. Their results show that the cross-section for *inelastic* scattering has *approximately* the value:

$$\sigma_i = \pi(r_n + \lambda\!\!\!^{-})^2, \tag{15}$$

where $\lambda\!\!\!^{-}$ is the deBroglie wave length divided by 2π. One can understand the physical significance of Eq. (15) by considering that the uncertainty principle assigns to a neutron of momentum p a "size" of the order of $\hbar/p = \lambda\!\!\!^{-}$ so that the interaction radius of this neutron with a nucleus of radius r_n is $r_n + \lambda\!\!\!^{-}$.

7.8. *Discussion of the experimental results on neutron scattering by complex nuclei.* The experimental data summarized in Table 7.2.1 show that the cross-sections of all nuclei decrease gradually with increasing neutron energy. The interpretation of the nuclear interactions of high-energy neutrons outlined in the preceding section offers a simple qualitative explanation for this phenomenon. In fact, from the experimental results presented in §§ 7.3, 7.4 and 7.5 one concludes that, as the neutron energy increases, the average cross-section, $\bar{\sigma}$, for its collisions with nucleons of the target nucleus decreases. Therefore nuclear matter becomes gradually more "transparent" to the incident neutron.

Indeed, it seems that the model of the semitransparent nucleus accounts quantitatively for the experimental results obtained with neutrons of less than about 100 Mev energy. This is shown by the fact that the radii of the various nuclei computed on the basis of this model are closely proportional to $A^{1/3}$, in agreement with Eq. (7.6.1) [(AE46); (FS49); (DJJ50.1); see also (FH49)].

As an example, Fig. 1 shows the nuclear radii obtained by DeJuren and Knable (DJJ50.1) from their measurements on the total scattering cross-sections of nuclei for 95-Mev neutrons. The slope of the straight line representing r_n as a function of $A^{1/3}$ corresponds to $r_0 = 1.38 \cdot 10^{-13}$ cm. In their computations, DeJuren and Knable used the value: $l_c = 3.33 \cdot 10^{-13}$ cm for the mean free path in nuclear matter. One may compare this value of l_c with the values of the cross-sections for collisions between free nucleons. As explained in the preceding section, a neutron incident upon a nucleus with 95 Mev kinetic energy has an energy of $95 + V_0 \approx 128$ Mev inside the nucleus. From Fig. 7.3.1 one obtains a value $\sigma_{np} \approx 6 \cdot 10^{-26}$ cm^2 for

the scattering cross-section of neutrons of this energy on free protons. If one assumes that $\sigma_{nn} = \sigma_{pp}$ one obtains from the same figure an approximate value $\sigma_{nn} = 2.5 \cdot 10^{-26}$ cm² for the scattering cross-section of 128-Mev neutrons on free neutrons. As mentioned in § 7.7, the exclusion principle makes the cross-sections relative to bound nucleons smaller than those relative to free nucleus. With this correction the cross-sections for the elementary interactions become: $\sigma_{np} = 4.4 \cdot 10^{-26}$ and $\sigma_{nn} = 1.9 \cdot 10^{-26}$.

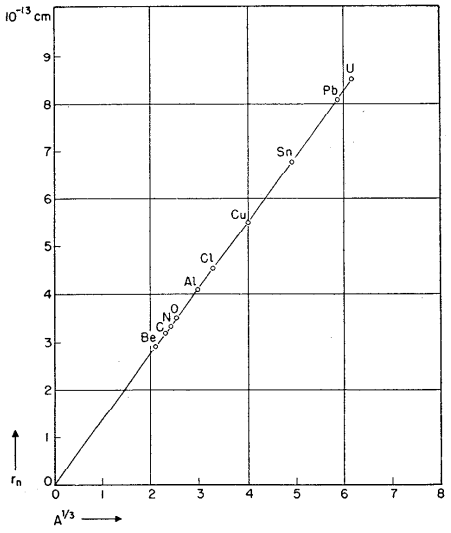

Fig. 7.8.1. Nuclear radii deduced from measurements of the total nuclear cross-sections for neutron scattering at 95 Mev, and plotted against the cubic roots of the mass numbers. The straight line represents the function $r_n = 1.38\ A^{1/3} \times 10^{-13}$ cm. From DeJuren and Knable (DJJ50.1).

The corresponding value of the mean free path in nuclear matter is $l_c \approx 3.8 \cdot 10^{-13}$ cm in the heaviest nuclei, for which $Z/A \approx 0.4$, and $l_c \approx 3.5 \cdot 10^{-13}$ cm in the nuclei of lower mass number, for which $Z/A \approx 0.5$. These values of l_c are slightly greater than the value used in the computations of DeJuren and Knable; but one must consider that σ_{nn} is known only crudely and that the computation of the nuclear cross-sections is not very sensitive to the value of l_c.

Elastic scattering of neutrons by nuclei was observed first by Amaldi and his collaborators (AE46) with 14-Mev neutrons and later by Bratenhal

and his collaborators (BtA50) with 84-Mev neutrons. The latter experimenters compared their results with the theory of Fernbach, Serber, and Taylor mentioned in § 7.7 and found satisfactory agreement.

Direct determinations of the *inelastic* scattering cross-sections are available for several nuclei (BtA50; DJJ50.1). These determinations were made by means of "poor-geometry" absorption measurements, whose principle is illustrated in Fig. 2. The absorber A, in the form of a truncated cone, is placed in a wide parallel beam of neutrons. The detector, D, is placed near the vertex of the cone. The aperture of the cone, θ_m, is chosen sufficiently large so that the probability of elastic scattering through angles greater than θ_m is negligible. One can prove that, under these conditions, the number of neutrons that are deflected away from the detector by elastic scattering very nearly equals the number of neutrons that are deflected toward the detector by the same phenomenon. Thus the decrease in the detected neutron flux corresponding to a given increase of the absorber thickness is entirely due to inelastic collisions in the added absorbing material. Inelastic collisions result either in outright absorption or in strong energy degradation of neutrons. If the detector has a sufficiently high energy threshold, practically no inelastic scattered neutrons will be detected and the measurement will give directly the mean free path for inelastic collisions.

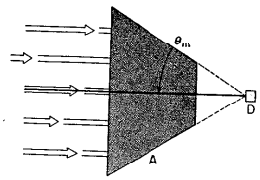

Fig. 7.8.2. Schematic experimental arrangement for a "poor geometry" absorption measurement.

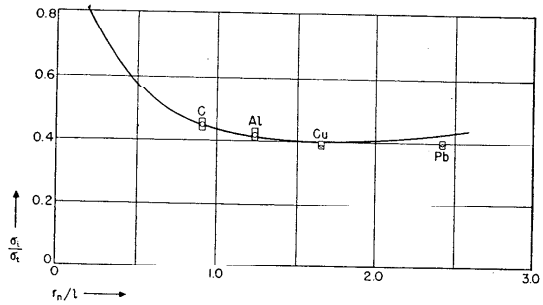

Fig. 7.8.3. Theoretical and experimental values of the ratio between inelastic and total scattering cross-sections of 95-Mev neutrons for several nuclei, plotted against the ratio of the nuclear radius to the mean free path in nuclear matter. From DeJuren and Knable (DJJ50.1).

Figure 3 shows the results obtained by DeJuren and Knable (DJJ50.1) from a comparison between "poor-geometry" absorption measurements (giving the *inelastic* cross section) and "good-geometry" absorption measurements (giving the total, i.e., the elastic plus inelastic cross-section). Neutrons were produced by stripping of 190-Mev deuterons and were detected with a bismuth fission chamber. The threshold of this detector was sufficiently high to insure that practically no inelastically scattered neutrons would be recorded. The estimated effective energy of the neutrons was 95 Mev. In Fig. 3 the abscissa represents the ratio r_n/l_c of the nuclear radius to the mean free path in nuclear matter, the ordinate is the ratio, σ_i/σ_t, between the inelastic and the total scattering cross-sections. The points are experimental determinations and the curve is computed from the theory of Fernbach and his collaborators (FS49) with $l_c = 3.3 \cdot 10^{-13}$ cm. One sees that the agreement is quite satisfactory.

Despite the success of the model of the "semitransparent" nucleus in explaining some of the experimental results on elastic and inelastic scattering of high-energy neutrons, one should not yet place undue confidence in the adequacy of the theory based upon this model. Indeed, this theory, at least in its simplest form, does not seem to account satisfactorily for the experimental data on the nuclear collision cross-sections of 270-Mev neutrons (DJJ51). It is not clear at the time of this writing how serious the disagreement is and how deep a modification of the theory it may require.

7.9. ***Nuclear disintegrations induced by high-energy nucleons.*** Inelastic collisions of nucleons with energies of the order of 100 Mev or more result, as a rule, in nuclear disintegrations of a more varied and complex nature than the nuclear disintegrations induced by nucleons of lower energy. These disintegrations give rise to groups of ionizing particles, mainly protons, occasionally heavier nuclear fragments. In photographic emulsions and in cloud-chamber pictures the disintegration products form characteristic patterns known as "stars." An example of such stars is shown in Fig. 1.

One can understand the essential features of the observed interactions on the basis of the same nuclear model that has been used in the previous sections for the interpretation of the experimental results on the scattering cross-sections (SbR47.2; GML48). Consider, for example, a high-energy neutron incident upon a nucleus. The neutron may collide against a nucleon and transfer part of its energy to it. The two nucleons resulting from the collision may escape from the nucleus without further collision, or may collide again with nuclear particles. At each new collision, an energy degradation occurs and the mean free path in nuclear matter of the secondary nucleons is correspondingly smaller than that of the parent nucleon.

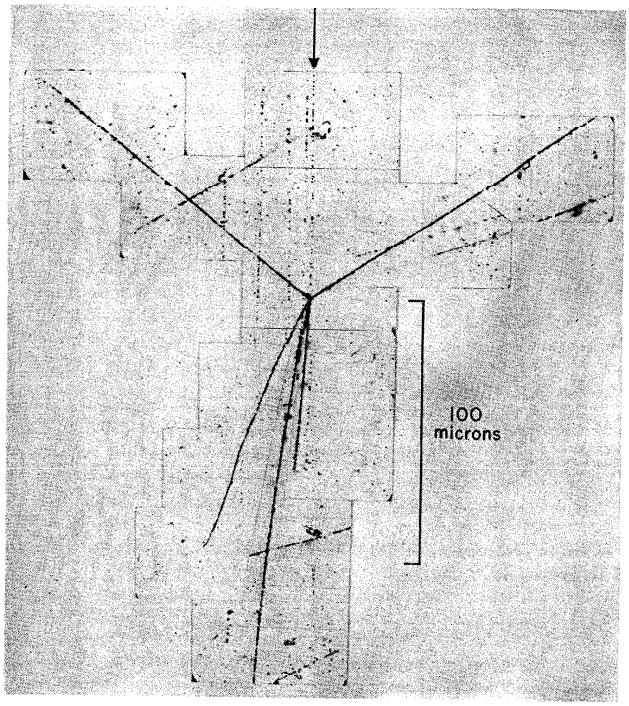

Fig. 7.9.1. Nuclear star produced in photographic emulsion by a fast proton (indicated by the arrow) from the Berkeley cyclotron; (courtesy of H. Bradner).

If, by chance, several collisions take place a short distance from one another it may happen that all of the particles resulting from these collisions have such small energies as to remain temporarily trapped in the nucleus. In this case the energy of the incident neutron goes entirely into nuclear excitation.

More frequently, however, the incident neutron, perhaps changed into a proton, will come out of the nucleus with reduced energy. Sometimes it will be accompanied by one or more secondary nucleons knocked out of the nucleus by direct collisions. When this happens, part of the incident energy will be found as kinetic energy of the nucleons coming out of the

nucleus immediately, while the rest will remain in the nucleus as excitation energy.

The excitation energy results partly from the kinetic energy of the nucleons that have undergone a collision but have not acquired enough energy to escape immediately, partly from the presence of "holes" left behind by the ejected nucleons. In a very short time the excitation energy of the nucleus will distribute itself in a statistical manner among all nuclear particles. In other words, the "temperature" of the nucleus as a whole will increase and, as a consequence, some of the nuclear particles will evaporate.

The above considerations lead one to picture a nuclear disintegration initiated by a high-energy nucleon as a two-step process.

The first step consists of the direct emission from the nucleus of one or several nucleons of comparatively high energy, including perhaps the incident nucleon itself. Heavier nuclear fragments, e.g., deuterons, may also be ejected [(YrH49); for a theoretical discussion of this effect, see (CGF50.3)]. The direct disintegration process occurs in a time of the order of the nuclear diameter divided by the velocity of the incident nucleon; i.e., in a time of the order of 10^{-22} sec. For a given energy of the incident nucleon, the number and the energy distribution of the ejected particles is determined, essentially, by the differential cross-sections for nucleon-nucleon scattering, by the number of nucleons in the target nucleus, and by their kinetic energy.

The second step consists of the evaporation of the residual nucleus. This evaporation occurs with a delay of the order, perhaps, of 10^{-21} sec. Most of the evaporated particles are neutrons, protons, and α-particles. The average energy of the emitted particles is of the order of 10 Mev; their number and their energy distribution is determined by the "temperature" of the nucleus; i.e., by the amount of energy that remains in the nucleus after the initial stage of the disintegration is completed.

It is hardly necessary to point out that a separation of the disintegration process into two sharply divided phases represents an idealization that is better justified in the case of heavy nuclei than in the case of light nuclei. Indeed, a light nucleus is likely to break up completely before equipartition of the energy among the nuclear particles occurs.

The evaporation process may be treated as a problem of statistical thermodynamics. A crude theory leads to the following expression for the energy spectrum of the neutrons emitted (WVF37):

$$N(E)\,dE = \text{const} \cdot \frac{E}{T^2}\, e^{-E/T}\, dE. \tag{1}$$

In this equation $N(E)\,dE$ represents the number of neutrons with energy in dE at E and T is the temperature of the nucleus measured in the same units as the energy E. For charged particles (protons, α-particles), Eq. (1) is replaced by the following:

$$N(E)\,dE = \text{const} \cdot \frac{E - V_0'}{2}\, e^{-(E-V_0')/T}\, dE, \tag{2}$$

where V_0' represents the height of the Coulomb barrier, again measured in energy units. (On the subject of the evaporation theory, see also § 8.10).

The initial phase of the disintegration, i.e., the direct emission of nucleons from the struck nucleus, can be analyzed by the "Monte Carlo" method, already mentioned in § 5.23. This method follows in detail the successive collisions of nucleons in nuclear matter, letting chance choose among the various possible effects of each elementary interaction and determine where such interaction occurs.

Goldberger (GML48) investigated the behavior of 100 neutrons of 86-Mev energy incident upon lead nuclei by the "Monte Carlo" method. He found that 15 neutrons went through the nucleus without a collision. This compares with a transparency of about 18 per cent, as computed from Eq. (7.7.10) with the values for the nuclear radius ($r_n = 9 \cdot 10^{-13}$) and for the collision mean free path in nuclear matter ($l_c = 6.2 \cdot 10^{-13}$) used by Goldberger (these values are different from those adopted in our previous discussion). Table 1 gives the number and the energy distribution of the emitted nucleons, as well as the excitation energy of the residual nucleus, for the remaining 85 cases.

One sees from this table that the average excitation energy of the residual nucleus is about 40 Mev. Similar computations by Bernardini and his collaborators for incident protons of 400 Mev energy gave a value of

Table 1.9.1. Theoretical results obtained by Goldberger (GML48) for 100 neutrons of 86-Mev energy incident upon lead nuclei. [15 pass through the nucleus without collision. The table describes the events occurring in the other 85 cases. All energies are in Mev. The three last columns give the average energy of the fastest, the second fastest and the third fastest particle coming out of the interaction.]

No. Particles Emerging	No. of Cases	Average Excitation Energy of Residual Nucleus	Average Energy of Emerging Particles		
			1	2	3
0	4	94.5			
1	58	41.6	45.0		
2	21	35.2	27.2	16.0	
3	2	40	14.5	9.5	6.5

80 Mev for the average excitation energy of the residual nucleus.* One sees that the average excitation energy increases, but only slowly, with increasing primary energy.

Table 1 also shows that many of the nucleons directly ejected from nuclei bombarded with 86-Mev neutrons have fairly low energies, so that they cannot be distinguished, on an energy basis, from the nucleons emitted during the subsequent evaporation process. According to Bernardini and his collaborators* this is also true in the case of disintegrations initiated by nucleons of several hundreds Mev energy.

Figures 2 and 3 describe some statistical data on nuclear stars produced in Ilford G5 electron-sensitive emulsions by protons of 400-Mev energy. In the evaluation of these data one should consider that most of the observed events represent disintegrations of the heavy nuclei contained in the emulsion (bromine and silver).

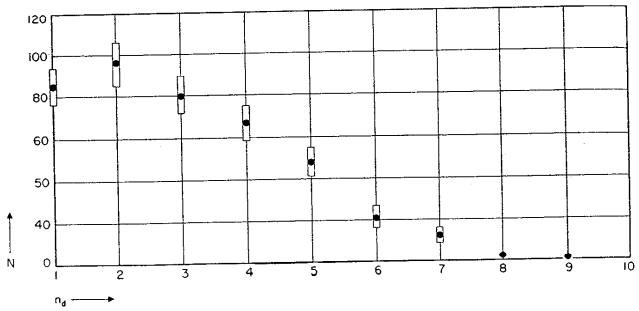

Fig. 7.9.2. The number, N, of stars with different numbers, n_d, of "dense" tracks produced in Ilford G5 emulsion by protons of energy between 350 and 400 Mev. Dense tracks are here defined as those with grain density greater than that of a 30-Mev proton. Private communication from G. Bernardini, E. T. Booth, and S. Lindenbaum.

Figure 2 shows the distribution of stars according to number of tracks with grain density greater than that of 30-Mev protons (these, incidentally, are the only tracks detected by electron-insensitive emulsions).

Figure 3 gives the percentage of events resulting in the emission of a proton with more than 30 Mev or with more than 100 Mev energy among stars with different numbers of dense tracks (grain density *greater* than that of a 30-Mev proton). One sees that the probability for the emission of a "fast" proton becomes smaller as the number of "slow" particles increases. One can easily understand this result by considering that, in the experiment under consideration, the available energy is the same

* Private communication from G. Bernardini to the author, January 1951.

in all cases. When a large fraction of this energy is carried away by fast secondary nucleons emitted during the initial stage of the disintegration, the excitation energy of the residual nucleus is small and so is the number of slow nucleons emitted during the evaporation process.

Both Fig. 2 and Fig. 3 clearly show that the phenomena initiated by the arrival of nucleons of a given energy upon nuclei are subject to large statistical fluctuations. In agreement with the theoretical predictions, one sees

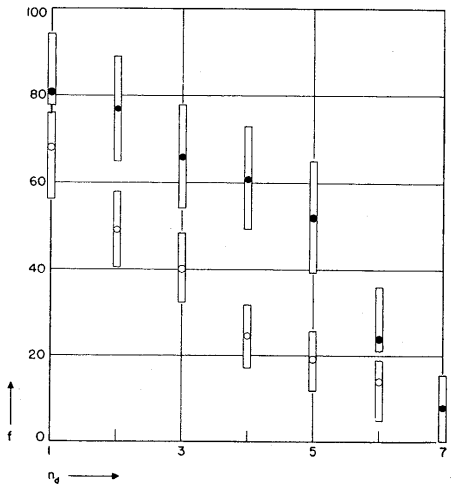

Fig. 7.9.3. The percentage, f, of stars containing the track of an outgoing proton with more than 30 Mev (black dots), or with more than 100 Mev (open circles), plotted as a function of the number, n_d, of "dense" tracks. Ilford G5 emulsion exposed to protons of energy between 350 and 400 Mev. Private communication from G. Bernardini, E. T. Booth, and S. Lindenbaum.

that sometimes the available energy is subdivided among a fairly large number of comparatively slow secondary particles; sometimes it is shared by a small number of fast secondary nucleons.

7.10. *Meson production in collisions between free nucleons.* In the nuclear interactions that we have discussed so far, the elementary event is an *elastic* collision between two nucleons; i.e., a collision in which the sum of the kinetic energies of the participating particles remains constant.

A nucleon of sufficiently high energy, however, may also collide *inelastically* with another nucleon, expending part of its kinetic energy in the production of one or more charged or neutral π-mesons.†

In Chapter 4 we have already mentioned the existence of this process. Symbolically the meson-producing interactions are represented by equations of the type:

$$p + p \rightarrow p + n + \pi^+, \tag{1a}$$

$$p + n \rightarrow p + p + \pi^-, \tag{1b}$$

$$p + n \rightarrow n + p + \pi^0. \tag{1c}$$

The threshold for meson-production is determined by the rest energy, $m_\pi c^2$, of the mesons and by the conservation laws of energy and momentum. In particular, these laws rule out the possibility that a nucleon of kinetic energy equal to $m_\pi c^2$ may come to rest on colliding against a free nucleon at rest and expend all of its kinetic energy in the production of a π-meson.

Let us first consider the collision in the frame of reference in which the center of mass of the two colliding nucleons is at rest. Let E^* be the kinetic energy of each nucleon in this frame of reference (we neglect here the small mass difference between proton and neutron). Let E be the kinetic energy of the incident nucleon in the frame of reference in which the target nucleon is at rest. This frame of reference practically coincides with the laboratory system if the target nucleon is a nucleus of hydrogen. If the target nucleon belongs to a complex nucleus, however, its velocity cannot be disregarded (see § 7.6). In the non-relativistic approximation:

$$E = 4E^*. \tag{2}$$

In order to obtain the exact relation between E^* and E, consider that for any system of particles, the difference between the square of the total energy and the square of the momentum times c is an invariant (see Appendix 2b). Therefore the following equation holds:

$$(E + 2Mc^2)^2 - c^2p^2 = (2E^* + 2Mc^2)^2, \tag{3}$$

where p is the momentum of a nucleon of kinetic energy E. With the help of Eq. (A.2.5), Eq. (3) yields:

$$E = 4E^*\left[1 + \frac{E^*}{2Mc^2}\right]. \tag{4}$$

The corresponding relation for the total energies of the incident particle, U and U^*, is:

$$M^2c^4 + Mc^2U = 2(U^*)^2. \tag{5}$$

† The words "elastic" and "inelastic" are used here with a meaning different from that used in the preceding sections, where we have described a collision between a nucleon and a nucleus as "inelastic" when part of the energy of the incident nucleon goes into exciting or disrupting the target nucleus.

In the center-of-mass system, the two nucleons may lose all of their kinetic energy in the production of a single meson at rest because the total momentum of the particles participating in such a process is zero both before and after the collision. Thus meson production may occur if $2E^* \geqslant m_\pi c^2$; i.e., if E is greater than the value E_0 given by the equation:

$$E_0 = 2m_\pi c^2\left[1 + \frac{m_\pi}{4M}\right]. \tag{6}$$

The quantity E_0 represents the threshold energy for meson production by protons or neutrons on hydrogen. If one uses the value $m_\pi c^2 = 141$ Mev for the rest energy of π-mesons (see § 4.13), one obtains for E_0 the value:

$$E_0 = 293 \text{ Mev}. \tag{7}$$

When meson production occurs at the threshold energy, the two colliding nucleons and the produced mesons are left at rest in the center-of-mass system. Therefore in the laboratory system the three particles move in the forward direction with the same velocity. The quantity $\frac{1}{2}m_\pi c^2$, representing the *initial* kinetic energy of each nucleon *in the center-of-mass system*, also represents the kinetic energy of each nucleon *after the collision, in the laboratory system*. In this system the kinetic energy of the π-meson, E_π, is given by the equation:

$$E_\pi = \frac{m_\pi}{M}\frac{m_\pi c^2}{2}, \tag{8}$$

and is thus approximately equal to 11 Mev.

When the energy of the incident nucleon is greater than E_0, only a portion of the kinetic energy available in the center-of-mass system goes into the production of the meson mass. After the collision, the π-meson and the two nucleons share the residual energy in such a way that the momenta of the three particles add vectorially to zero in the center-of-mass system. This condition does not determine the energy of the meson uniquely. Therefore mesons produced at energies above threshold have a continuous energy distribution, both in the center-of-mass system and in the laboratory system.

In the center-of-mass system, the kinetic energy of the meson is a maximum when, after the collision, the two nucleons have equal and parallel momenta. The momentum of the meson is then equal in magnitude and opposite in direction to the combined momentum of the two nucleons. On the other hand, the sum of the kinetic energies of the three particles is $(2E^* - m_\pi c^2)$. In the non-relativistic approximation, one thus obtains the following expression for the maximum kinetic energy of the meson in the center-of-mass system:

$$(E_\pi^*)_{\max} = \frac{2M}{2M + m_\pi}(2E^* - m_\pi c^2). \tag{9}$$

Consider now, in particular, the production of positive mesons in the proton-proton collisions described by Eq. (1a). If one ignores the interaction between the proton and the neutron resulting from each collision of this kind, one predicts for the produced mesons a fairly uniform energy spectrum extending from zero to the maximum allowed energy. However, the attraction between proton and neutron favors a final state in which the two nucleons have approximately equal and parallel momenta, so that they may remain temporarily in the vicinity of one another. If this effect is important, one may expect, in the center-of-mass system, an energy distribution for the π-mesons strongly peaked at the upper end, i.e., near $(E_\pi)_{\max}$.

Indeed the neutron and the proton may combine to form a deuteron:

$$p + p \rightarrow d + \pi^+. \tag{10}$$

In this case the kinetic energy available after the reaction is greater than that available after the reaction (1a) by an amount equal to the binding energy of the deuteron:

$$W_d = 2.2 \text{ Mev}.$$

Thus reaction (10) produces, in the center-of-mass system, a mono-energetic group of mesons of energy:

$$(E_\pi^*)_d = \frac{2M}{2M + m_\pi}(2E^* - m_\pi c^2 + W_d). \tag{11}$$

In the laboratory system the energy of the mesons resulting from this reaction is not unique, but is uniquely determined by the angle of emission.

Members of the Berkeley group have investigated the production of charged mesons in the collisions between free protons by bombarding

Table 7.10.1. Experimental values of the differential cross-section for meson production by proton-proton interaction at various angles to the incident beam. [Primary energy: 345 Mev. Cross-sections in units of 10^{-28} cm^2 sterad^{-1}. Laboratory system.]

Angle	Differ. Cross-section	Observors
0°	2.0 ± 0.4	Cartwright, Richman, Whitehead, and Wilcox
18°	$1.6 \pm \begin{matrix}0.24\\0.08\end{matrix}$	Peterson, Hoff, and Sherman
30°	0.58 ± 0.07	Peterson, Hoff, and Sherman
60°	0.08 ± 0.04	Richman and Whitehead

polyethylene $[(CH_2)_n]$ or liquid hydrogen with the external proton beam of the 184-inch cyclotron (CWF50; PV50). In the first experiment they determined the meson yield of hydrogen by taking the difference between the meson yields of a polyethylene target and of a carbon target containing the same number of carbon atoms. In both experiments the detector consisted of photographic plates embedded in absorbers of aluminum or copper. Observation of meson tracks ending in the emulsions of the various plates gave information on the number of mesons that came to rest at various depths in the absorbers and thus determined the energy distribution of the incident mesons.

Figure 1 shows the experimental arrangement used by Cartwright, Richman, Whitehead, and Wilcox (CWF50) in their study of meson production in polyethylene and carbon. The arrangement was designed to permit the observation of mesons produced in the forward direction. For this purpose, positive and negative mesons were separated from the direct proton beam by a magnetic field and fell upon the detectors after passing through suitable channels cut in a large shielding block. The ion chamber placed in the path of the incident proton beam served to measure the intensity of this beam, thus making an absolute determination of cross-sections possible.

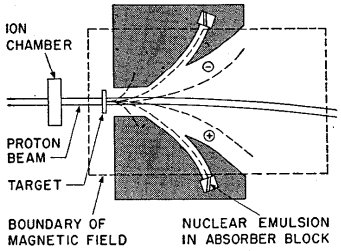

Fig. 7.10.1. The experimental arrangement used by Cartwright *et al.* (CWF50) to observe the production of positive π-mesons by protons.

As anticipated, the experimental results showed that all charged mesons produced in proton-proton encounters are positive.

In the forward direction (CWF50) as well as at 30° from the incident beam (PV50), the energy spectrum of the produced mesons was found to be characteristically peaked at the high-energy end. This is illustrated in Fig. 2, giving the differential cross-section for the production of mesons of different energies by 345-Mev protons in the forward direction.

The shape of the meson spectrum shows that the resonance attraction between proton and neutron in the final state plays a very important role in the process of meson production. However, it is not possible to determine from the data summarized in Fig. 2 whether or not the reaction leading to the bound deuteron state actually occurs. For a primary energy of 345 Mev this reaction should produce in the forward direction a mono-energetic group of mesons of about 74 Mev energy. The maximum energy of the mesons that arise from a collision leaving the proton

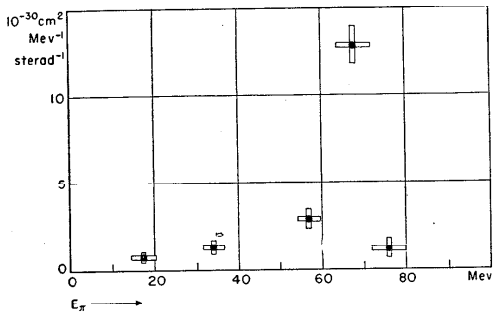

Fig. 7.10.2. The energy distribution of positive π-mesons produced by 345-Mev protons on protons in the direction of the beam. The quantity plotted as abscissa is the meson energy E_π in Mev. The quantity plotted as ordinate is the absolute value of the differential cross-sections per steradian and per Mev. From Cartwright *et al.* (CWF50).

and neutron in an unbound state is about 70 Mev. If the reactions (1a) and (10) occur simultaneously, one should thus observe, in the forward direction, a 4-Mev "gap" near the upper end of the meson spectrum. The energy resolution achieved in the experiments under discussion was not sufficient to decide whether or not this gap exists.*

Table 1 shows some preliminary results obtained by the Berkeley group on the angular distribution of π^+-mesons produced by proton-proton interaction at 345 Mev energy.†

The total cross-section for π^+-meson production by protons on protons at 345 Mev is approximately:

$$\sigma_{\pi^+} \approx 2 \cdot 10^{-28} \text{ cm}^2. \tag{12}$$

No information is available as yet as to the dependence of this cross-section on energy.

Crandall, York, and Moyer explored the possibility that *neutral* mesons may be produced in the collisions between two protons, according to the reaction:

$$p + p \rightarrow p + p + \pi^0. \tag{13}$$

This experiment gave a negative result and was sufficiently accurate to establish the fact that the cross-section for neutral meson production is at least ten times smaller than the cross-section for positive meson production.‡

* Later experiments have demonstrated the simultaneous production of deuterons and π^+-mesons by the collisions of protons with protons, and have thus proved that reaction (10) actually occurs [(CFS51)]; see also [(CWF51)].

† Private communication by W. F. Cartwright to the author, February 1951.

‡ Private communication to the author, January 1951.

7.11. ***Meson production in the collisions of nucleons with complex nuclei.*** The interpretation of the experiments on the production of mesons in the collisions of nucleons against complex nuclei is quite difficult. The fundamental process is probably still an interaction between the incident nucleon and one of the nucleons of the nucleus. However, the nuclear structure affects the result of this interaction considerably, at least when the incident energy is not very large.

Consider first the problem of the threshold energy for meson production. In discussing this question one must take into account primarily the following factors: (1) the motion of the nucleons in the nucleus; (2) the exclusion principle; and (3) the possibility that the nucleus as a whole may acquire some momentum.

If one describes the nucleus as a Fermi gas (see § 7.6) one finds that the maximum kinetic energy, E_f, of the bound nucleons is about 25 Mev and their corresponding momentum, p_f, is about 216 Mev/c. For a given momentum of the incident nucleon, the energy available for meson production is a maximum when this nucleon collides against a bound nucleon coming directly toward it with momentum p_f. In the non-relativistic approximation meson production becomes energetically possible when the momentum of each colliding nucleon in the center-of-mass system is greater than the momentum, p_0, determined by the condition:

$$2\frac{p_0^2}{2M} = m_\pi c^2. \tag{1}$$

This equation gives $p_0 \approx 360$ Mev/c. For the head-on collision considered above, the corresponding momentum of the incident nucleon in the laboratory system is:

$$2p_0 - p_f \approx 500 \text{ Mev/c}. \tag{2}$$

However, one can easily see that the exclusion principle rules out the possibility of meson production by a nucleon of 500 Mev/c momentum colliding with a nucleon of momentum $-p_f$. In fact, after the collision, both nucleons should be at rest in the center-of-mass system. Hence their momentum in the laboratory system should be $(500 - 216)/2 \approx 140$ Mev/c. This momentum is smaller than p_f and therefore corresponds to an already occupied quantum state.

One thus concludes that, at least in the case of medium and heavy nuclei, where the Fermi model is applicable, the actual threshold for meson production is not determined by the conservation of momentum and energy in the nucleon-nucleon collisions, but rather by the exclusion principle. This principle states that the number of nucleons with kinetic energy less than the Fermi energy cannot increase as a result of the interaction. Therefore the process of meson production that requires least energy of the incident nucleon is one in which this particle, after the collision, remains in the nucleus with a kinetic energy equal to E_f. In this

process the energy going into meson production equals the initial kinetic energy of the nucleon plus the binding energy of this nucleon in the nucleus, $E_B \sim 8$ Mev. One then obtains the following expression for the threshold energy, E'_0:

$$E'_0 = m_\pi c' - E_B \approx 133 \text{ Mev}. \tag{3}$$

As noted above, in the process of meson production, the nucleus as a whole may acquire some momentum. If the nucleus is sufficiently heavy, the corresponding kinetic energy is negligible.*

The collision of a proton with a proton, as already pointed out, gives rise only to positive mesons; meson production may occur with either one of the colliding protons changing into a neutron. The collision of a proton with a neutron, instead, may give rise to a positive meson (with the proton changing into a neutron) as well as to a negative meson (with the neutron changing into a proton). These considerations suggest that in a p-n collision there is equal probability for the production of positive and negative π-mesons, and that the probability of positive π-meson production is twice as large in a p-p collision as in a p-n collision.

Since light nuclei contain approximately equal numbers of protons and neutrons one might expect that the bombardment of light nuclei with protons should yield three times more positive than negative mesons. This conclusion, however, is correct only at the limit of large energies. In the low-energy region the positive-to-negative ratio is drastically affected by the nuclear structure. In the first place, the Coulomb barrier that surrounds the nuclei hinders the emission of positive mesons of low energy and therefore decreases the positive-to-negative ratio. Also, the exclusion principle decreases the probability of certain reactions more strongly than that of others (see ref. CGF50.1).

Consider, for example, the two processes:

$$p + n \rightarrow p + p + \pi^-,$$
$$p + n \rightarrow n + n + \pi^+.$$

In the first case, *both* of the resulting protons must have energies greater than the Fermi energy, since all lower energy states of protons are occupied. In the second case, however, only one of the two resulting neutrons need have an energy greater than the Fermi energy, while the other may remain in the same energy state that it occupied before the collision. Thus the first process is less likely to occur than the second, even though both processes would have the same probability if the target neutron were free. One sees that the exclusion principle tends to increase the positive-to-negative ratio in the case of proton bombardment and tends to decrease this ratio in the case of neutron bombardment. The effect of the exclusion

* For a more detailed discussion of the threshold energy see refs. (MMW47) and (BWH49).

principle, as well as that of the Coulomb barrier, becomes less pronounced as the incident energy increases. Therefore one should expect the positive-to-negative ratio to be strongly energy-sensitive.

Experiments on the production of mesons by collisions of nucleons with complex nuclei confirm, qualitatively at least, the general conclusions reached above. In particular, these experiments show that the threshold for meson production is much lower when the target material contains complex nuclei than when it consists of pure hydrogen. The actual value of the threshold energy is difficult to determine experimentally because the excitation curve near threshold rises very slowly with increasing energy. Meson production, however, has been definitely detected, in carbon, at a proton energy of 200 Mev (JSB50).

The experimental values of the positive-to-negative ratio are roughly of the expected order of magnitude and exhibit roughly the expected energy dependence [see refs. (RC50; BH50.2)]. The absolute yields of positive, negative, and neutral mesons are consistent with the values of

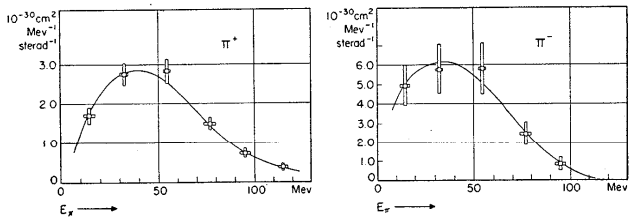

Fig. 7.11.1. The differential cross-sections, in the laboratory system, for the production of positive and negative π-mesons by 345-Mev protons in carbon, plotted against meson energy. Angle of observation: 90° ± 12° to the direction of the beam. From Richman *et al.* (RC50).

the cross-sections for meson production in the collisions between free nucleons, as modified by the exclusion principle and by the Coulomb barrier. (One should note also, of course, that the bound deuteron state is no longer favored as the end product of a p-p collision when the target proton belongs to a complex nucleus.) In particular, the rate of production of neutral mesons by protons seems to indicate that these mesons are produced only in the collisions of the incident protons with the neutrons of the target nucleus. One must emphasize, however, that neither theory nor experiment is sufficiently accurate to justify any quantitative conclusion at the present time.

As an example of the experimental results mentioned above, Fig. 1 shows the differential cross-sections for the production of positive and

negative π-mesons by 345 Mev protons on carbon at 90° from the beam, as measured by Richman and Wilcox (RC50).

7.12. *Meson production by γ-rays in hydrogen.* Experiments have shown that high-energy γ-rays are capable of producing charged and neutral π-mesons through reactions that may be represented symbolically as follows:

$$\gamma + p \rightarrow n + \pi^+, \tag{1a}$$

$$\gamma + n \rightarrow p + \pi^-, \tag{1b}$$

$$\gamma + p \rightarrow p + \pi^0, \tag{1c}$$

$$\gamma + n \rightarrow n + \pi^0. \tag{1d}$$

Since, according to our previous conclusions, π-mesons have integer spin, these reactions are consistent with the principle of conservation of spin.

Consider first the production of mesons by photons in hydrogen, represented by Eq. (1a). In order to compute the threshold for this effect we shall consider again the interaction in the "center-of-mass system," i.e., in the system where the incident photon and the target proton have equal and opposite momenta. In this system the energy of the photon plus the initial energy of the proton equals, at the threshold, $m_\pi c^2 + Mc^2$. Therefore the threshold energy, E_0, in the frame of reference in which the proton is at rest is given by the equation:

$$(E_0 + Mc^2)^2 - E_0^2 = (m_\pi c^2 + Mc^2)^2, \tag{2}$$

from which it follows:

$$E_0 = m_\pi c^2 \left[1 + \frac{1}{2}\frac{m_\pi}{M}\right], \tag{3}$$

or:

$$E_0 \approx 152 \text{ Mev}. \tag{4}$$

At thresholds, the π-meson is produced at rest in the center-of-mass system. In the laboratory system it travels in the direction of the incident γ-ray beam with a velocity equal to that of the recoil nucleon. The meson and the recoil nucleon share the energy $E_0 - m_\pi c^2$ in proportion of their respective masses. From Eq. (3) it thus follows that the kinetic energy of the meson has the value:

$$E_\pi = \frac{1}{2} m_\pi c^2 \frac{m_\pi}{M} \cdot \frac{m_\pi}{M + m_\pi} \approx 1.4 \text{ Mev}. \tag{5}$$

Photons with energies greater than the threshold energy produce mesons of different energies in the laboratory system. However, since only two particles are present at the end of the process, the energy of a meson is uniquely determined by its angle of emission and by the energy of the incident photon. Conversely, mesons observed in a given direction and with a given energy are all produced by photons of the same energy even though photons of many different energies may be present in the incident beam.

In hydrogen, photons can produce only positive or neutral mesons. The production of *positive* mesons in hydrogen has been investigated by Bishop, Steinberger, and Cook (BAS50)* with the following experimental method. The γ-ray beam of the Berkeley synchrotron operated at 322 Mev passes through a vessel containing liquid hydrogen. The mesons produced in the hydrogen are detected by means of "telescopes," each consisting of three scintillation crystals that will be denoted as 1, 2, and 3 in order of increasing distance from the target (see Fig. 1). Electronic circuits select those simultaneous pulses of crystals 1 and 2 that are *not* accompanied by a pulse in crystal 3 and that are followed by a second pulse in crystal 2 with a delay of the order of microseconds. An event of this type characterizes a π^+-meson traversing the first crystal, coming to rest in the second crystal, and then producing, by successive disintegrations, a μ-meson and an electron. The recorded delay corresponds to the $\mu \rightarrow e$ disintegration (the $\pi \rightarrow \mu$ disintegration is not resolved in this experiment). By means of appropriate absorbers, placed between the target and the telescope, it is possible to select mesons belonging to definite energy intervals, whose width is determined essentially by the thickness of the crystal No. 2 where the mesons are required to stop.

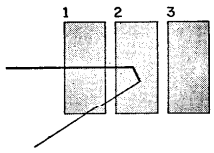

Fig. 7.12.1. Schematic illustration of an experimental arrangement used for the detection of positive π-mesons. The π-meson traverses crystal 1, stops in crystal 2 where it produces, by successive disintegrations, a μ-meson and an electron.

The γ-radiation from a synchrotron source has a continuous energy distribution and therefore produces, in each direction, mesons of different energy. However, as already noted, for each direction of observation, there is a unique correspondence between the energy of the primary photon and that of the secondary meson. Thus one can single out a practically mono-energetic group of photons by properly selecting the energy of the mesons (this energy, of course, will be different for the different directions).

With this method Bishop and his collaborators obtained some data on the angular distribution of π^+-mesons produced by 250-Mev photons. These data are shown in Fig. 2. Monitoring of the incident meson beam made it possible to measure the differential cross-section in absolute value and therefore to obtain, by integration, a crude value of the total cross-section for π^+-meson production at 250 Mev. This value is approximately $2 \cdot 10^{-28}$ cm^2 (see footnote on page 384).

Figure 3 gives the meson yield at 90° from the γ-ray beam in the laboratory system as a function of photon energy. The evaluation of the

* Earlier experiments carried out by means of a different method are described in ref. (SJ50.1).

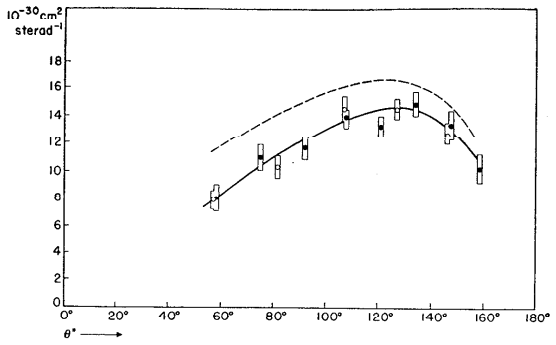

Fig. 7.12.2. The differential cross-section in the center-of-mass system for the production of π^+-mesons by 250-Mev photons in hydrogen. Open circles represent the results of experiments with liquid hydrogen described in the text. Black dots represent the results of earlier experiments, in which the hydrogen effect was obtained by a subtraction method. The standard errors indicated refer to the relative values. The estimated error in the absolute values of the cross-sections is +20%, −10%. Appropriate absorbers select, in the different directions, mesons of different energies, corresponding to the same energy of the primary photons. Some of the mesons undergo nuclear interactions in the absorber. The dashed line represents the experimental data corrected for this effect (under the assumption of geometric cross-section). From Bishop, Steinberger, and Cook (BAS50).*

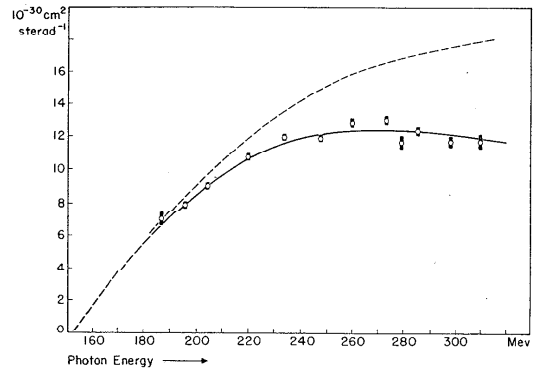

Fig. 7.12.3. The differential cross-section in the laboratory system for the production of positive π-mesons in hydrogen by photons of various energies, at 90° to the beam. The errors indicated refer to the relative values. The estimated error in the absolute values is +20%, −10%. The dashed line represents the experimental results corrected for the effect of nuclear interactions of π-mesons in the absorbers (see caption to Fig. 7.12.2.). From Bishop, Steinberger and Cook (BAS50).*

* According to a private communication from Steinberger to the author (March 1952), the ordinates in Figs. 2 and 3 should be multiplied by 1.8.

data plotted in this figure is based upon the knowledge of the energy spectrum of photons in the synchrotron beam (see § 6.2) and upon the relation between meson energy and photon energy mentioned above. The yield appears to increase steadily with increasing photon energy, but the slope of the excitation curve seems to become gradually smaller.

Steinberger, Panofsky, and Steller (SJ50.2, SJ350) investigated the production of *neutral mesons* in hydrogen by means of the experimental arrangement already described in § 4.15 (see Fig. 4.15.3) which detects the photon pairs arising from the decay of neutral mesons.

Preliminary results indicate that the excitation function for neutral meson production by the γ-p interaction starts with zero slope at threshold and then increases rapidly with increasing energy. It thus differs markedly from the excitation function for positive meson production (see Fig. 3). In absolute value, the cross-sections for neutral and positive meson production by γ-rays on hydrogen are the same within a factor of two at 320 Mev.

7.13. *Meson production by γ-rays in complex nuclei.* The production of mesons by photons in complex nuclei is affected by the same factors (exclusion principle, Coulomb barrier, motion of the nucleons) that have already been mentioned in the discussion of meson production by protons. There is, however, some experimental indication that the dependence on atomic number of the cross-section for meson production by photons is strongly influenced by another factor, not considered previously; i.e., by the opacity of nuclear matter to π-mesons.

Nuclear matter is very transparent to γ-rays; therefore meson production occurs with equal probability in the whole nuclear volume. If π-mesons could escape from the nuclei unimpeded, the nuclear cross-section for the production of π^+-mesons should increase in proportion to Z (apart from the perturbing effect of the Coulomb barrier) and the nuclear cross-section for the production of π^0-mesons should increase in proportion to A. If, instead, π-mesons are strongly absorbed in nuclear matter, then only mesons produced near the surface of the nuclei can escape. At the limit for very large opacity of nuclear matter, the probability of escape of a π-meson will vary in proportion to the ratio of the nuclear surface to the nuclear volume; i.e., in proportion to $1/A^{1/3}$.

Figure 1 summarizes some preliminary experimental data on the cross-sections of various nuclei for the production of positive and neutral mesons by photons.* The experiment consisted of irradiating targets of various elements with the γ-ray beam of the Berkeley synchrotron operated at 322 Mev, and measuring the yields of positive and neutral mesons at 90° from the beam. In Fig. 1, the abscissa represents $1/A^{1/3}$. The ordinate represents the observed yield of positive mesons divided by Z, or the observed yield of neutral mesons divided by A. Both yields are expressed in terms of the meson yields of a hydrogen target containing the same

* Private communication from Steinberger, Steller, and Panofsky to the author, January 1951. The data on charged mesons were obtained by Mozley (MRF50).

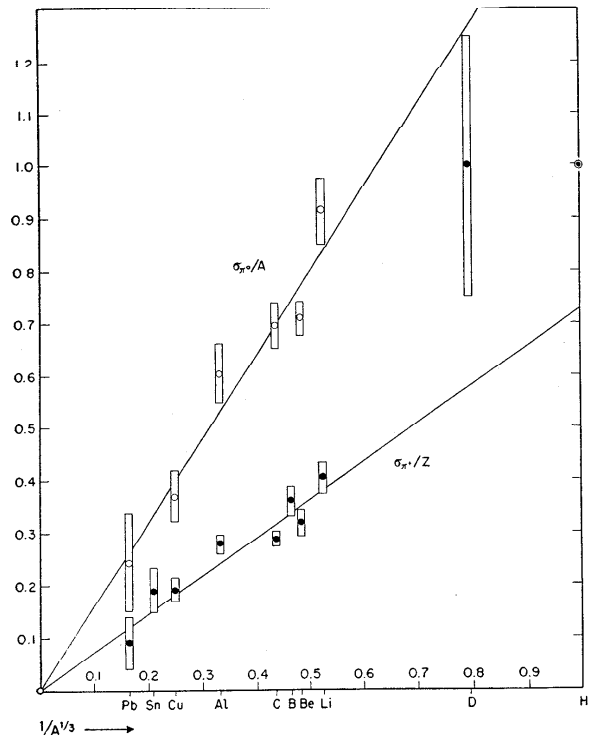

Fig. 7.13.1. The cross-section per nucleon for the production of neutral mesons (σ_{π^0}/A), and the cross-section per proton for the production of positive mesons (σ_{π^+}/Z) by γ-rays in various nuclei. Data taken at 90° to the γ-ray beam and normalized to 1 at the hydrogen cross-section. The abscissa is the inverse cubic root of the atomic mass number. The errors shown are the statistical deviations. Private communication from W. K. H. Panofsky to the author.

number of nuclei as the specimen in question. In the limiting case of perfectly "transparent" nuclei, the points corresponding to the various elements should lie on horizontal lines. In the limiting case of perfectly "opaque" nuclei, they should lie on straight lines passing through the origin. It is very remarkable that the experimental points should follow so closely the curve predicted theoretically for perfectly opaque nuclei.

We feel, however, that any definite conclusion, based on these preliminary results, would be premature.

7.14. ***Nuclear interactions of π-mesons from artificial sources.*** Bernardini and his collaborators (BG50; BG51.1; BG51.2) have reported some interesting observations of nuclear interactions by negative π-mesons in Ilford G5 emulsions. The π-mesons were produced by the Columbia cyclotron; their energy was from 30 to 50 Mev in the earlier experiments, from 70 to 90 Mev in the later experiments. We present here some of the results relative to mesons of the higher-energy group.

By following individual meson tracks through the emulsion, the authors detected a number of nuclear interactions, which they classified as follows:

(a) *Stars:* the π-meson disappears and produces a nuclear disintegration;

(b) *Inelastic scattering:* the π-meson survives; either it is slowed down so that the grain density of the outgoing meson track is at least three times that of the incoming track, or it produces a nuclear disintegration;

(c) *Elastic scattering:* the π-meson trajectory is deflected by more than 20°, with a change of energy of less than 30 Mev (if any); there is no visible nuclear disintegration;

(d) *Stopping:* the π-meson disappears in flight without producing any visible nuclear disintegration.

Table 1 shows the distribution of the observed events among the three categories. One should notice that only a small fraction of the events classified as elastic scattering may be ascribed to Coulomb interaction. About half of them, however, are probably cases of "diffraction scattering" (see § 7.7).

From the total length of π-meson track explored and the number of interactions observed, one can determine the collision mean free path of π-mesons in the emulsion. According to Bernardini and his collaborators, the mean free path for all nuclear interactions is 18 ± 4 cm. If one disregards diffraction scattering, the mean free path is somewhat greater than the figure quoted above and is not significantly different from the geometric mean free path.

Table 7.14.1. Classification of the nuclear interactions produced by π^--mesons of 70 to 90 Mev energy in Ilford G5 emulsions. [From Bernardini *et al.* (BG51.1).]

Stars	Inelastic Scattering	Elastic Scattering	Stopping
20	6	11	4